RESEARCH TRIANGLE INSTITUTE

RTI/5294/92-Quarterly

November 1992

HETEROEPITAXIAL DIAMOND GROWTH

Quarterly Report -- Second Quarter
1 July 1992 - 30 September 1992

R. J. Markunas
R. A. Rudder
R. E. Thomas
J. B. Posthill
G. C. Hudson

STRATEGIC DEFENSE INITIATIVE ORGANIZATION
Innovative Science and Technology Office

Office of Naval Research
Program No.
N00014-92-C-0081

POST OFFICE BOX 12194 RESEARCH TRIANGLE PARK, NORTH CAROLINA 27709-2194

REPORT DOCUMENT PAGE

Form Approved
OMB No 0704-0188

1. AGENCY USE ONLY *(Leave blank)*	2. REPORT DATE	3. REPORT TYPE AND DATES COVERED
	November 1, 1992	Quarterly Report July 1, 1992 -- September 30, 1992

4. TITLE AND SUBTITLE

Heteroepitaxial Diamond Growth

5. FUNDING NUMBERS

N00014-92-C-0081

6. AUTHOR(S)

R. J. Markunas, R. A. Rudder, J. B. Posthill, R. E. Thomas, G. Hudson

7. PERFORMING ORGANIZATION NAME(S) AND ADDRESS(ES)

Research Triangle Institute
P. O. Box 12194
Research Triangle Park, NC 27709

8. PERFORMING ORGANIZATION REPORT NUMBER

83U-5294

9. SPONSORING/MONITORING AGENCY NAME(S) AND ADDRESSES(ES)

Office of Naval Research
800 N. Quincy Street
Arlington, VA 22217-5000

10. SPONSORING/MONITORING AGENCY REPORT NUMBER

11. SUPPLEMENTARY NOTES

12a. DISTRIBUTION/AVAILABILITY STATEMENT

Approved for public release; unlimited distribution

12b. DISTRIBUTION CODE

13. ABSTRACT

Work during this phase of the diamond program began to focus on issues which were limiting diamond technology:

1) The role of oxygen in diamond CVD,
2) Why the limited success of heteroepitaxy on Ni?
3) Tools for quantitative microstructural characterization
4) Techniques for separation and lift-off of thin single crystal sheets of diamond
5) Epitaxial consolidation of individual diamond crystals,
6) High quality homoepitaxy.

Highlights of this period include expounding the role of O in diamond CVD through surface chemistry, expounding the role of subsurface species to CH_3 adsorption on Ni(111) surfaces, developing ion implantation annealing procedures for separation of thin diamond platelets, plan-view TEM characterization of type Ia and IIb diamonds, epitaxial consolidation of two adjacent diamonds, and critical evaluation of H_2/CH_4, $H_2/CH_4/CO$, H_2/CO chemistries for homoepitaxial growth.

14. SUBJECT TERMS

15. NUMBER OF PAGES

16. PRICE CODE

17. SECURITY CLASSIFICATION OF REPORT	18. SECURITY CLASSIFICATION OF THIS PAGE	19. SECURITY CLASSIFICATION OF ABSTRACT	20. LIMITATION OF ABSTRACT
UNCLASSIFIED	UNCLASSIFIED	UNCLASSIFIED	

TABLE OF CONTENTS

1.0 Program Activity 1
2.0 Ongoing Informal Collaborations 3
3.0 Publications and Presentations 6

1.0 PROGRAM ACTIVITY

Work during this phase of the diamond program began to reap the fruits of the collaborations established during the first quarter. Many details of the formal and informal collaborations were given in the previous quarterly report. Consequently, we will only report on the highlights of the collaborations. As discussed in the previous report, the diamond program at RTI pursued two separate avenues for large area single-crystal diamond development:

1) diamond heteroepitaxy,
2) diamond bonding, consolidation, and lift-off.

Congruent with those approaches, workers here at Research Triangle Institute identified key issues which needed to be addressed before progress could be realized. Those issues, in turn, dictated classes of experimental and theoretical activity. The issues and the classes of activity are listed below:

1) the role of oxygen in diamond CVD,
   a) surface chemistry studies: LEED, TPDS, AES,
   b) theoretical calculations to ascertain the oxygen site(s), b) CVD growth with oxygen-containing gasses,
   c) SIMS analysis for impurity content,

2) why the limited success of diamond heteroepitaxy on Ni,
   a) theoretical modeling of CH_3 adsorption on Ni (the role of subsurface impurities (catalyst),
   b) ion implantation for controlled introduction of subsurface impurities (catalyst),
   c) low temperature diamond growth,

3) tools for quantitative microstructural characterization,
   a) TEM sample preparation,
   b) spatially resolved catholuminescence,
   c) chemical etching for defect delineation,
   d) Atomic Force Microscopy (atomic resolution),

4) techniques for separation and lift of thin single crystal sheets of diamond
   a) C^+ and O^+ implantations,
   b) determination of implant range and straggle,

c) temperature activated separation techniques,

5) epitaxial consolidation of individual crystals into one single crystal (Details of bonding not yet patent secured),

6) high quality diamond homoepitaxy for the epitaxial consolidation
   a) microstructural comparison of available growth chemistries,
   b) development of novel plasma sources for higher rate, larger area diamond deposition.

These activities have generated some very exciting results. Almost all these activities have involved very active collaboration between staff at RTI and the both the formal and informal subcontractors. Many joint publications and paper submissions have occurred during this quarter. Those papers (reproduced in section 3.0) are included in this quarterly report to provide a comprehensive record of this work.

2.0 ONGOING INFORMAL COLLABORATIONS

In addition to the informal collaborations with Penn State described in 1st quarterly report, TEM Studies at RTI have been facilitated by excellent collaborative work with Jet Propulsion Laboratory (JPL). Two important things have been accomplished thus far in our collaboration with Dr. Thomas George and Dr. Tom Pike at JPL. They were able to make a cross-section TEM sample of a diamond layer grown on Si using a CF_4/H_2 mixture. This particular grown sample was notable because diamond nucleated readily on the Si substrate *without* any substrate pretreatment (e.g., diamond scratching) whatsoever. There were 2 "interlayers" observed on this sample - the first (closest to the diamond) was a 150 nm thick region of polycrystalline β-SiC. Beneath that layer was an amorphous layer of varying thickness (it was not uniform) which averaged ~ 1.5 μm. Although this result is not completely understood, it is encouraging that there is no apparent interlayer between the SiC and the diamond, which may warrant nucleation studies on single crystal β-SiC using halogen-containing diamond growth chemistries for possible heteroepitaxy.

Single crystal diamond were sent by RTI to JPL for the purpose of JPL developing a rapid, laser-based method of making plan-view TEM samples. The crystals were natural type Ia diamonds, and the technique developed is to be used ultimately to examine the details of the microstructure of CVD-grown homoepitaxial diamond films. Using the pulsed excimer laser to "burn" from one side of the diamond has been successful. Final thinning was then accomplished in their ion mill and TEM micrographs were obtained. A manuscript detailing the application and methodology of this technique is being prepared by Dr. Thomas George. We plan to soon use this technique on homoepitaxial diamond that is currently being grown.

In addition, cross-section TEM results have been obtained on diamond grown on Si in the presence of copper. At the diamond growth temperature, the Cu vapor pressure is quite substantial (~ 10^{-6} Torr), thereby providing a continuous overpressure and supply of Cu to the nucleating surface and to the diamond growth. It was found that polycrystalline diamond grown on Si in the presence of Cu was showed a much smoother surface topography and an apparently smaller grain size. This was using a more traditional CH_4/H_2 gas mixture. JPL has made a cross-section TEM sample and made initial examination of it. It appears as if there are very small nodules of a 3rd phase at the diamond/Si interface, and efforts have begun to identify them. Possibilities include a Cu silicide phase or SiC. JPL researchers took the TEM sample to the High Resolution Electron Microscopy facility at Arizona State University, but due to equipment problems, did not get a final answer. Time is being scheduled to make another attempt to get this microanalytical result.

Complementing the TEM studies Cathodoluminescence (CL) studies have been undertaken at RTI in conjunction with both Arizona State University and AT&T Bell Laboratories.

EBIC and panchromatic CL images taken in the SEM at RTI of natural type IIb single crystal diamond indicated that dislocations were arranged in a cellular structure and were electrically active and luminescent, indicating that dislocations are associated with states in the gap that can be responsible for light emission in the visible and IR. The states may be intrinsic to the dislocations themselves, or combine with impurities present to create the states. Individual dislocations were not resolved due to the small spacing (avg. ~ 0.5 μm) and relatively large electron beam interaction volume diameter (~ 4 μm at 25KeV). TEM on the same stone verified that the dislocations were "clustered" into cells. A portion of this same stone was sent to Dr. Gene Fitzgerald at AT&T Bell Labs in the context of a non-contractual collaboration. CL date was collected in his SEM at low

temperature (6 °K) and was found to be strongest at 430nm, which has been associated with donor-acceptor recombination due to nitrogen and boron impurities, respectively. Other CL peaks were observed at 589nm, 648nm, and 680nm. Again, it is anticipated that this initial work done on a natural crystal will be extended to homoepitaxial diamond in the following phase of the program.

Collaboration (non-contractual) with Dr. Roger Graham at Arizona State University (ASU) in the area of TEM-based high spatial resolution CL has continued at a low level. Of most interest is the his results on polycrystalline diamond grown using water:alcohol:acetic acid mixtures. Using CL mapping, initial results appear to indicate that characteristic CL lines associated with nitrogen are significantly more intense in regions that are rich in microtwins/stacking faults. If this result turns out to be verified by further experiment, it could imply that N may play a role in the extensive twinning/faulting that is so characteristic of polycrystalline diamond. Additionally, a thin layer (~ 2 μm) that has been implant lifted-off from a type Ia diamond has also been sent to ASU and has been specially (locally) thinned using focused ion milling. Dr. Graham has made initial TEM examination, and has found the layer to remain single crystal. A full microstructural and CL analysis has yet to be done on this sample.

Finally, in the area of "Super" SIMS Studies: North Texas State University, there has been continued contact and discussion with Prof. Floyd McDaniel in the Physics Department of North Texas State University. A water:methanol diamond homoepitaxial film was sent to Floyd McDaniel for initial experimentation and trial of his more sensitive "super" SIMS techniques. This sample was of particular interest because it showed the lowest N and O concentration by measurement with conventional SIMS. However, it is recognized that a more sensitive technique for particularly the presence of N will be needed. Upon discussions, it is clear that equipment difficulties have inhibited progress to date for this characterization.

3.0 PUBLICATIONS AND PRESENTATIONS

1. *Effects of Subsurface Na, H and C on CH_3 Adsorption on Ni(111)*, H. Yang, J.L. Whitten, R.E. Thomas, R.A. Rudder, and R.J. Markunas.

2. *Single Crystal Diamond Plate Lift-Off Achieved by Ion Implantation and Subsequent Annealing*, N.R. Parikh, J.D. Hunn, E. McGucken, M.L. Swanson, C.W. White, R.A. Rudder, D.P. Malta, J.B. Posthill, and R.J. Markunas.

3. *Formation of Diamond Films from Low Pressure Radio Frequency Induction Discharges*, R.A. Rudder, G.C. Hudson, R.C. Hendry, R.E. Thomas, J.B. Posthill, and R.J. Markunas.

4. *Hydrogen-Oxygen Exchange Reactions on Diamond(100) Surfaces*, R.E. Thomas, R.A. Rudder, and R.J. Markunas.

5. *Surface Processes During Diamond Growth from Water-Alcohol Vapor rf-Plasma Discharges*, R.E. Thomas, R.A. Rudder, G.C. Hudson, and R.J. Markunas.

6. *The Effect of Local Carbon Sources on Diamond Nucleation*, R.A. Rudder, G.C. Hudson, J.B. Posthill, and R.J. Markunas.

7. *Growth and Characterization of SiGe Contacts on Semiconducting Diamond Substrates*, T.P. Humphreys, P.K. Baumann, K.F. Turner, R.J. Nemanich, K. Das, R.G. Alley, D.P. Malta, and J.B. Posthill.

8. *A Correlative Investigation of Defects in Natural and PECVD-Grown Diamond*, D.P. Malta, J.B. Posthill, E.A. Fitzgerald, R.A. Rudder, G.C. Hudson, and R.J. Markunas.

9. *Homoepitaxial Diamond Layers Grown with Different Gas Mixtures in a rf Plasma Reactor*, J.B. Posthill, D.P. Malta, R.A. Rudder, G.C. Hudson, R.E. Thomas, and R.J. Markunas.

10. *Diamond Surface Studies of Growth Mechanisms from Water-Alcohol Deposition Chemistries*, R.E. Thomas, R.A. Rudder, and R.J. Markunas.

11. *Low Temperature Diamond Growth: Development of Water-Based Techniques for Diamond CVD*, R.A. Rudder, R.E. Thomas, G.C. Hudson, J.B. Posthill, D.P. Malta, and R.J. Markunas.

12. *Nucleation of Diamond Films on Non-Native Substrates*, J.B. Posthill, D.P. Malta, R.E. Thomas, G.C. Hudson, and R.J. Markunas.

Surface Science Letters 277 (1992) L95–L99
North-Holland

surface science letters

Surface Science Letters

Effects of subsurface Na, H and C on CH_3 adsorption on Ni(111)

Hong Yang, Jerry L. Whitten
Department of Chemistry, North Carolina State University, Raleigh, NC 27695-8204, USA

Raymond E. Thomas, Ronald A. Rudder and Robert J. Markunas
Research Triangle Institute, Research Triangle Park, NC 27709-2194, USA

Received 26 June 1992; accepted for publication 6 August 1992

Ab initio valence orbital configuration interaction calculations are used to study the energy effect of Na, H and C atom subsurface species on CH_3 chemisorption at a hollow 3-fold site on Ni(111). The lattice is modeled as an embedded three layer cluster of 41 atoms. Ni 3d orbitals are explicitly included on seven nickel atoms on the surface. The calculated chemisorption energies of pyramidal CH_3 on Ni(111) are 38 for the clean surface and 50, 47, and 17 kcal/mol for the Na, H, and C implants, respectively. The energies required to distort tetrahedral CH_3 into a planar structure are 22 kcal/mol on clean Ni(111), 30 kcal/mol with the Na implant, 24 kcal/mol with the H implant, and 12 kcal/mol with the C implant, respectively. Thus, Na below the surface may stabilize a carbon overlayer to a tetrahedral diamond structure. CH_3–surface distances, C–H stretching and surface–CH_3 vibrational frequencies are also reported.

1. Introduction

In the past decade, diamond film growth has received a great deal of attention not only due to the pure scientific interest in the low pressure formation of metastable diamond but also due to the many practical applications that exist for diamond films [1–9]. Despite the progress that has been made in developing a variety of techniques for diamond film formation, understanding the mechanisms for diamond formation is still a subject of current debate. Continued progress in diamond film technology will depend in particular on developing a better understanding of diamond heteronucleation and correspondingly heteroepitaxy. Heteroepitaxial growth of diamond on c-BN has been successful, but the availability of c-BN limits the utility of this technology. Epitaxial growth on other closely lattice matched materials such as Ni, Cu, or Co have had only limited success. The formation of aligned diamond crystals in a small local area has been reported for diamond growth on Ni [10]. One difficulty in diamond heteroepitaxy is the poor chemical bonding between adsorbate and substrate. During heteronucleation, adsorbate species such as methyls are receiving substantial fluxes of atomic H. Under this high flux, carbon adsorbates on the surface are gasified, defeating diamond nucleation. As a result, diamond nucleation and growth is sporadic and highly three-dimensional.

In the present studies, ab initio cluster model calculations are used to investigate the energy effect of subsurface interstitials such as Na, H, and C on the bonding of a CH_3 radical to a hollow 3-fold site on Ni(111). The calculated results show that the presence of electropositive subsurface species in Ni dramatically increase the bond strength between a CH_3 radical and the Ni surface. Correspondingly, electronegative subsurface species such as C dramatically weaken a CH_3–Ni surface bond. In addition, the energy required to planarize a tetrahedral CH_3 on Ni(111) increases when electropositive species reside interstitially below the Ni surface.

Calculations are performed in the context of a many-electron embedding theory that permits the accurate computation of molecule–solid surface interactions at an ab initio configuration interaction level. The CH_3 and local surface region are treated as embedded in a lattice electron distribution which is modeled as a 41-atom, three layer cluster.

The objective of the present paper is to calculate the adsorption energy of CH_3 on Ni(111) with subsurface Na, H, and C implants and then to calculate the energy required to distort the tetrahedral CH_3 into a planar structure on the surface.

2. The theory and calculations

The purpose of the embedding theory employed in this work is to treat adsorbed species and a surface region of the metal with sufficient accuracy to describe reaction energetics, while at the same time maintaining a proper coupling of the surface region to the bulk [11–13]. The present approach most closely resembles that in refs. [14,15], where the details of the method are discussed. Calculations are performed by first obtaining self-consistent-field (SCF) solutions for the nickel cluster plus adsorbed species. The occupied and virtual orbitals of the SCF solution are then transformed separately to obtain orbitals spatially located about all the atoms of the cluster except those in the seven-atom surface region shown in fig. 1. This unitary transformation of orbitals is based upon exchange maximization with the valence orbitals of atoms outside the surface region and is designed to enhance convergence of the configuration interaction (CI) expansion [11–13].

The CI calculations involve single and double excitations from multiple parent configurations within a 28 or 29-electron subspace to 28 possible localized virtual orbitals. All configurations arising from excitations with an interaction energy greater than 1×10^{-5} hartree with the parent SCF configuration are explicitly retained in the expansion; contributions of excluded configurations are estimated using second order perturbation theory. For all geometries calculated, the SCF solution is the dominant configuration. Configurations with coefficients > 0.05 are included as parent configurations. Details of the procedure are given in ref. [16]. Basis superposition contributions to the total energy were taken into account by calculating the energy of the Ni cluster with the adsorbed species' virtual basis present (but not the adsorbate nuclei).

The cluster geometry and local region of the nickel cluster used to model the (111) crystal face of nickel are shown in fig. 1. The three layer, 88-atom cluster, consists of a surface layer of 37

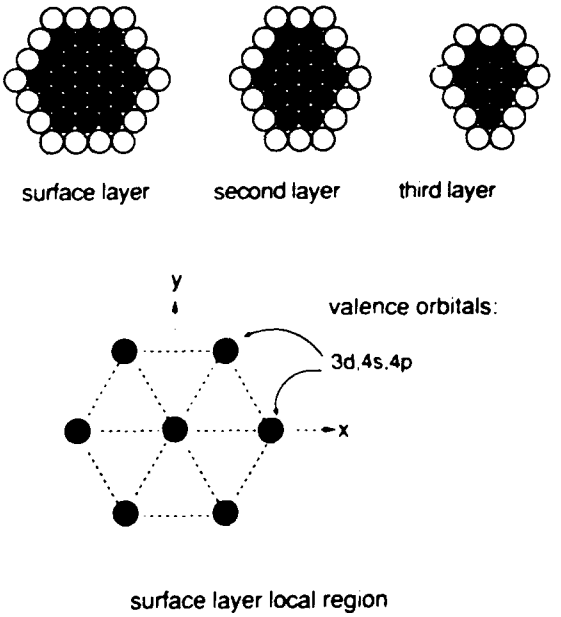

Fig. 1. Cluster geometry and local region of the nickel cluster used to model the (111) crystal face of nickel. The three layer, 88-atom cluster, consists of a surface layer of 37 atoms, a second layer of 30 atoms and a third layer of 21 atoms. Embedding theory is used to reduce the Ni_{88} cluster to a 41 atom model depicted as shaded atoms. Atoms surrounding the seven local region atoms in the surface layer and those surrounding the four central atoms in the second layer are described by effective potentials for $(1s)^2 \cdots (3p)^6(3d)^9(4s)^{1.2}$ and $(1s)^2 \cdots (3p)^6(3e)^9(4s)^{1.10}$ configurations, respectively. Effective potentials for the shaded atoms in the third layer describe the $(1s)^2 \cdots (3p)^6(3d)^9(4s)^{1.4}$ configuration. Unshaded atoms have neutral atom (1s–3p core)$(3d)^9(4s)^1$ potentials. All atoms have Phillips–Kleinman projectors $\Sigma |Q_m\rangle\langle Q_m| (-\epsilon_m)$ for the fixed electronic distribution. The nearest neighbor Ni–Ni distance is 2.48 Å.

atoms, a second layer of 30 atoms and a third layer of 21 atoms. Embedding theory is used to reduce the Ni_{88} cluster to the 41-atom model depicted as shaded atoms: the surface layer of 19 atoms, a second layer of 14 atoms, and a third layer of 8 atoms. For the seven-nickel-atom local surface region, a [1s–3p] core potential is used; 3d, 4s and 4p orbitals are explicitly included in the valence basis. Other Ni atoms are described by an effective core potential for [1s–3d] electrons, and a single 4s orbital. For all boundary atoms, and those in the third layer, the core potential is further modified to account for bonding to the bulk region, as described in refs. [14,15]. The basis orbitals of Ni, C, and H are the same as used in previous dissociative chemisorption studies of CH_4 on Ni(111) [17]. A double-zeta s and p basis for Na is taken from Veillard [18] and augmented with a set of p polarization functions (exponent of 0.5).

The Na, H and C interstitials are positioned below a hollow 3-fold site and midway between the first and second layers, as shown in fig. 2.

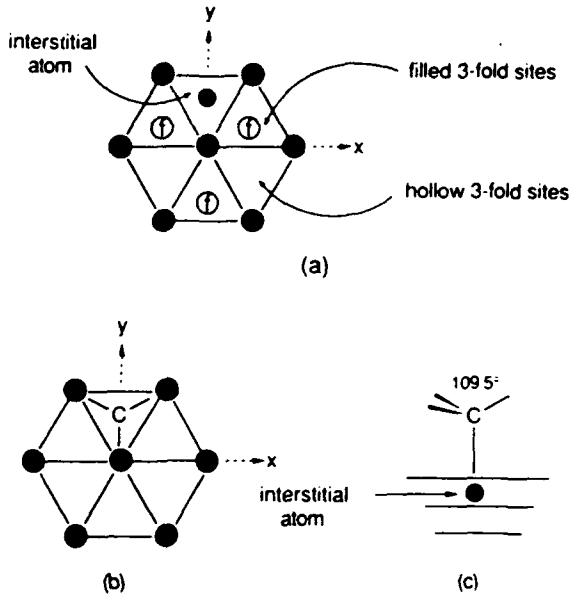

Fig. 2. CH_3 geometry and the local region of Ni(111) showing subsurface Na, H and C atoms. The interstitial species are below a hollow 3-fold site, midway between the first and second layers. The vertical distance of the interstitial to the first and second layers is 1.01 Å.

3. Results

Fig. 2 shows the geometry of pyramidal CH_3 adsorbed at a hollow 3-fold site, where there is no second layer Ni atom underneath. The interstitial Na, H or C atom is below the hollow 3-fold site, in the interstitial position midway between the first and second layers. In the initial carbon–surface distance optimization, the C–H bond lengths are fixed at 1.08 Å and the HCH angles at 109.5°. Calculated adsorption energies, distances from CH_3 to the surface, and vibrational frequencies are reported in table 1. For CH_3 on clean Ni(111), the computed adsorption energy is 38 kcal/mol with a surface–CH_3 distance of 1.90 Å. These values along with the calculated vibrational frequencies are consistent with our previous calculations of CH_3 on Ni(111), where the lattice was modeled as a 28-atom, three layer cluster [19,20].

For CH_3 adsorption at the 3-fold site above the interstitial atom, the chemisorption energy increases to 50 and 47 kcal/mol for Na and H subsurface atoms, respectively. However, the energy decreases to 17 kcal/mol in the case of a C subsurface atom. The distances of $CH_3$to the surface change only slightly from 1.85 to 1.93 Å.

Thus CH_3 adsorption energies are comparable for Na and H interstitials; while the subsurface C significantly weakens the CH_3–surface bond to a

Table 1
Adsorption energies (E_b), CH_3 distances from C to the surface (R_e), and vibrational frequencies for CH_3 adsorbed at a hollow 3-fold site on Ni(111) with subsurface Na, H and C interstitials.

	E_b (kcal/mol)	R_e (Å)	Ni–CH_3 stretch (cm^{-1})	C–H stretch (cm^{-1})
Ni(111)	38	1.90	374	3140
Na interstitial	50	1.85	361	3140
H interstitial	47	1.87	340	3130
C interstitial	17	1.93	476	3170

Results are from configuration interaction calculations and are corrected for basis superposition effects of approximately 3 to 4 kcal/mol.

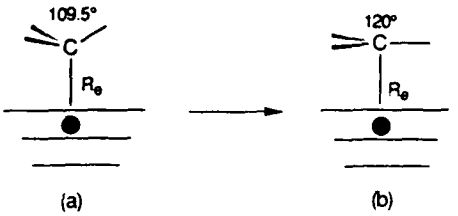

	Ni(111)	Na Interstitial	H Interstitial	C Interstitial
ΔE (Kcal/mol)	+22	+30	+24	+12

Fig. 3. Tetrahedral and planar CH_3 geometries on Ni(111) with subsurface Na, H and C interstitials (shaded circles). The interstitials are below a hollow 3-fold site, midway between the first and second layers. ΔE is the energy required to distort the tetrahedral geometry of (a) into a planar structure of (b). The CH_3-surface distances (R_e) are listed in table 1.

value less than one-half that for Ni(111) with no interstitial species. Na is an electron donor and the 3s electron is distributed over the neighboring Ni atoms in the first and second layers. It is therefore easier for CH_3 to receive electronic charge from the surface and form a strong bond. The interstitial H behaves somewhat like the Na interstitial, but its net charge is only $+0.09|e|$. On the other hand, Mulliken populations from the SCF calculations show that the C interstitial receives almost 2 electrons [21]. The surface adsorption region becomes electron deficient, and the CH_3-surface bond strength is diminished since it is more difficult for CH_3 to pull electrons from the substrate.

Fig. 3 shows the energy required to distort the tetrahedral CH_3 into a planar structure on Ni(111) with and without the interstitial species. The purpose of these calculations is to determine whether the implants stabilize or destabilize the CH_3 tetrahedral geometry. The figure shows that the energy required to distort tetrahedral CH_3 to a planar sp^2 geometry is 22 kcal/mol on Ni(111), at the surface-CH_3 equilibrium distance of 1.90 Å. For Ni(111) with an interstitial Na atom, this energy increases to 30 kcal/mol, for interstitial H, the value is 24 kcal/mol, and with the C interstitial atom, only 12 kcal/mol is required. The latter value is about one-half that required for distortion of CH_3 on Ni(111) with no implant.

As indicated above, the interstitial atoms are positioned below a hollow 3-fold site and midway between the first and second layers, i.e., at the center of an octahedral hole in the lattice. The smaller, tetrahedral hole (below the filled 3-fold site) was not investigated. The octrahedral hole is not quite large enough to accommodate Na^+ and is much too small for negatively charged carbon. Therefore, we would expect that interstitial species such as Na and C, and to a lesser extent hydrogen, will expand the lattice locally. This in turn will affect some of the properties we have calculated, but the extent is unclear. Further, the implant species are mobile and in the case of H and C may ultimately react with the adsorbed CH_3. Thus, although the large effects found in the present study are intriguing, much more work is needed before a quantitative understanding of accompanying effects will be possible.

4. Conclusions

The conclusions of the present study of CH_3 at a hollow 3-fold site on Ni(111) with subsurface Na, H and C interstitials can be summarized as follows.

(1) Tetrahedral CH_3 binds strongly to the Ni(111) when an interstitial Na or H atom implant is present; the adsorption energy is 50 or 47 kcal/mol, respectively, compared to 38 kcal/mol for Ni(111) with no implant. The adsorption energy is only 17 kcal/mol in the presence of a subsurface C implant. The corresponding CH_3-surface distances are 1.85, 1.87, and 1.93 Å for Na, H, and C cases, respectively. With no implant the value is 1.90 Å.

(2) Energies required to distort tetrahedral sp^3 CH_3 into a planar sp^2 structure are 22 kcal/mol on Ni(111), and 30, 24, and 12 kcal/mol for Na, H, and C implants, respectively.

(3) Calculated C–H stretching frequencies are all around 3150 cm^{-1} with or without the implants. The surface-CH_3 perpendicular stretch vibrational frequencies are 374 cm^{-1} on Ni(111), and 361, 340, and 476 cm^{-1} with the Na, H, and C implants, respectively.

(4) The present studies indicate that C below the Ni surface may make it easier for a carbon overlayer to revert to a planar graphite structure, while interstitial Na atoms may stabilize a tetrahedral C sp^3 structure on Ni(111).

Note added: A recent published experimental study by Ceyer and coworkers [22] has demonstrated that interstitial H is the active species in the hydrogenation of CH_3 on Ni(111). The reaction of surface hydrogen with methyl is inhibited by a substantial energy barrier [17]. The experimental evidence is consistent with H in an octahedral interstitial site reacting with CH_3 adsorbed at the 3-fold surface site above H (see fig. 2c). Our theoretical results suggest that the presence of interstitial H enhances the adsorption energy of CH_3 at this site.

Acknowledgments

This work was supported by the Office of Naval Research, the Strategic Defense Initiative Organization–Innovative Science and Technology office. Studies of the clean surface and interstitial H was supported by the US Department of Energy.

References

[1] R. Messier, J.T. Glass, J.E. Butler and R. Roy, Eds., New Diamond Science and Technology (MRS, Pittsburgh, 1991).
[2] R.F. Davis, Z. Sitar, B.E. Williams, H.S. Kong, H.J. Kim, J.W. Palmour, J.A. Edmond, J. Ryu, J.T. Glass and C.H. Carter, Jr., Mater. Sci. Eng. B 1 (1988) 77.
[3] R.A. Rudder, J.B. Posthill and R.J. Markunas, Electron. Lett. 25 (1989) 1220.
[4] K.E. Spear, J. Am. Ceram. Soc. 72 (1989) 171.
[5] H. Kawarada, J.S. Ma, T. Yonehara and A. Hiraki, Mater. Res. Soc. Symp. Proc. 162 (1990) 195.
[6] H. Itoh, T. Nakamura, H. Iwahara and H. Sakamoto, in: New Diamond Science and Technology, Eds. R. Messier, J.T. Glass, J.E. Butler and R. Roy (MRS, Pittsburgh, 1991) p. 929.
[7] W.A. Yarbrough, J. Vac. Sci. Technol. A 9 (1991) 1145.
[8] J.F. Prins and H.L. Gaigher, in: New Diamond Science and Technology, Eds. R. Messier, J.T. Glass, J.E. Butler and R. Roy (MRS, Pittsburgh, 1991) p. 56.
[9] J. Narayan, V.P. Godbole and C.W. White, Science 252 (1991) 416.
[10] Y. Sato, I. Yashima, H. Fujita, T. Ando and M. Kamo, in: New Diamond Science and Technology, Eds. R. Messier, J.T. Glass, J.E. Butler and R. Roy (MRS, Pittsburgh, 1991) p. 371.
[11] J.L. Whitten and T.A. Pakkanen, Phys. Rev. B 21 (1980) 4357.
[12] J.L. Whitten, Phys. Rev. B 24 (1981) 1810.
[13] P. Cremaschi and J.L. Whitten, Surf. Sci. 149 (1985) 273.
[14] J.L. Whitten, in: Cluster Models for Surface and Bulk Phenomena, Eds. G. Pacchioni and P.S. Bagus (Plenum, New York, 1992) p. 375.
[15] P. Cremaschi and J.L. Whitten, Theor. Chim. Acta 72 (1987) 485.
[16] P. Madhavan and J.L. Whitten, J. Chem. Phys 77 (1982) 2673.
[17] H. Yang and J.L. Whitten, J. Chem. Phys. 96 (1992) 5529.
[18] A. Veillard, in: Handbook of Gaussian Basis Sets, Eds. R. Poirier, R. Kari and I.G. Csizmadia (Elsevier, New York, 1985) table 11.9.2.
[19] H. Yang and J.L. Whitten, J. Am. Chem. Soc. 113 (1991) 6442.
[20] H. Yang and J.L. Whitten, Surf. Sci. 255 (1991) 193.
[21] The electron charge ascribed to the C atom (and to H or Na) should not be interpreted strictly as an atomic charge but as a measure of the electron distribution in the vicinity of the interstitial atom.
[22] A.D. Johnson, S.P. Daley, A.L. Utz and S.T. Ceyer, Science 257 1992) 223.

SINGLE CRYSTAL DIAMOND PLATE LIFT-OFF ACHIEVED BY ION IMPLANTATION AND SUBSEQUENT ANNEALING

N.R. Parikh, J.D. Hunn, E. McGucken, M.L. Swanson; University of North Carolina, Chapel Hill, NC 27599-3255;
C.W. White; Oak Ridge National Laboratory, Oak Ridge, TN 37831-6048;
R. A. Rudder, D.P. Malta, J.B. Posthill, R.J. Markunas; Research Triangle Institute, Research Triangle Park, NC 27709-2194.

ABSTRACT

We describe a new method for removing thin, large area sheets of diamond from bulk or homoepitaxial diamond crystals. This method consists of an ion implantation step, followed by a selective etching procedure. High energy (4 -5 MeV) implantation of carbon or oxygen ions creates a well-defined layer of damaged diamond that is buried at a controlled depth below the surface. For C implantations, this layer is graphitized by annealing in vacuum, and then etched in either an acid solution, or by heating at 550-600°C in oxygen. This process successfully lifts off the diamond plate above the graphite layer. For O implantations of a suitable dose ($3 \cdot 10^{17}$ cm^{-2} or greater), the lift-off is achieved by annealing in vacuum or flowing oxygen. In this case, the O required for etching of the graphitic layer is also supplied internally by the implantation. This lift-off method, combined with well-established homoepitaxial growth processes, has considerable potential for the fabrication of large area single crystalline diamond sheets.

An essential hurdle yet to be cleared, before one can fabricate diamond electronic devices, is the creation of large area, flat, single crystalline diamond layers. A very promising beginning has been made by Pryor et al.[1] ,who have shown that homoepitaxial diamond layers can be grown by chemical vapor deposition onto a matrix of oriented diamond microcrystallites, which are imbedded in an array of etch pits on a Si substrate. However, this method is both costly and time-consuming, and the crystallites are only poorly oriented, thus causing low angle grain boundaries We propose to combine homoepitaxial growth with lift-off technology to permit large area diamond sheets to be economically fabricated from a master template. For example, such diamond films could be fabricated by tiling together several small diamond crystals on which one then deposits a single crystalline layer; and then removing thin sheets of single crystalline diamond from the surface using a lift-off process. In this way, a large diamond template could be fabricated, from which large diamond sheets could be removed ad infinitum. In the present paper, we shall describe the use of ion implantation to lift thin sheets of diamond from a single crystal substrate.

In our lift-off method, we have used ion implantation to create a buried damaged layer in a polished bulk diamond crystal, and then removed that damaged layer by selective etching, thus lifting

a thin sheet of diamond from the surface. The fundamental concepts of the method are the following. (a.) Most of the damage caused by ion implantation occurs at the end of the ion range, and thus is confined to a buried layer of material at a controllable depth. (b.) The damaged layer can be graphitized by annealing, and the graphitized layer has sharp boundaries because of the well-defined critical damage density necessary for conversion of diamond to graphite [3,4]. (c.) The graphitic layer can be preferentially etched at a much more rapid rate than that of the adjacent diamond. We note that successful lift-off of $Al_xGa_{1-x}As$ films has been achieved by selectively etching a buffer layer of AlAs located between a GaAs substrate and the $Al_xGa_{1-x}As$ layer.[5] The etching of the damaged diamond can be achieved in different ways: for example, via reaction with oxygen supplied externally or internally, or by dissolution in an acid solution. We shall discuss results for both of these methods.

It is known[3,4] that ion beam damage caused by carbon implantation at low temperatures in diamond can be divided into four general regimes.

(i.) At low doses ($<1.5\cdot10^{15}$ C ions/cm^2 at 100 keV, corresponding to a Frenkel defect concentration of ~7%), the damage is almost completely recoverable by thermal annealing at about 900°C in vacuum.

(ii.) At doses $>1.5\cdot10^{15}$ C ions/cm^2 at 100 keV, a stable damaged diamond structure ("green diamond"[4]) may be formed by annealing at 950°C.

(iii.) At doses greater than about 10^{16} C ions/cm^2 at 100 keV, the damaged diamond is graphitized by thermal annealing at moderate temperatures (about 600°C).

(iv.) At very high doses, diamond is spontaneously graphitized. It should be noted, however, that diamond is much more resistant to such graphitization when the damaged layer is buried, perhaps because of the constraint on expansion due to the relatively undamaged overlying diamond[6].

The depth profile of ion beam damage can be calculated using Monte Carlo computer programs, such as TRIM[7]. Because high energy ions lose most of their energy via electronic collisions, there is relatively little damage near the surface of an ion-implanted sample. The damage is confined to a relatively narrow buried region near the end of the ion range, where the ions lose most of their energy via nuclear collisions. Thus, by varying the initial ion energy, the depth of the buried damaged layer can be controlled. The thickness of the buried damaged layer is almost independent of the ion energy. Consequently, a buried thin layer of graphite can be created in diamond by ion implantation followed by low temperature annealing.

Selective etching of the graphitic layer can be achieved by several methods.

(1.) Since a hot chromic-sulfuric acid solution etches graphite much more rapidly than diamond, it is apparent that lift-off could be achieved by the graphitizing of a buried layer followed by an acid etch. However, because the overlying diamond is also attacked by the etch, it would be necessary to first grow a thick diamond overlayer onto the implanted diamond. Also, the penetration of the acid into the narrow graphitic layer may be slow. In the case of removal of $Al_xGa_{1-x}As$ layers

by an HF etch, the penetration was aided by providing an overlayer that caused the $Al_xGa_{1-x}As$ layer to curl up at the edges during the etching[5].

(2.) The graphitic layer can be etched by annealing in an oxygen atmosphere[2]; i.e., burning the graphite to form CO or CO_2. It is important that the etching rate of the graphitic layer is considerably faster than the rate for diamond.

(3.) In method (2.), the oxygen must be supplied via diffusion from the edge of the sample. However, if the implanted species is oxygen, the implantation serves the dual role of creating the damaged layer and providing the required O for etching.

As an alternative to selective etching, the overlayer may be removed by mechanical shearing. In this case the damaged layer could be graphitic, or alternatively it could be a low shear resistant material created by implantation with ions which do not form volatile compounds.

Natural diamond type Ia and IIa crystals, in the form of polished thin plates 2x2 or 3x3 or 4x4 mm areal dimensions and 0.25 mm thick (from Dubbeldee Harris Diamond Corp.), were implanted with C^+ or O^+ ions to doses of $6 \cdot 10^{16}$ cm^{-2} to 10^{18} cm^{-2} at energies of 4 to 5 MeV. The ranges for 4 MeV C^+ and 5 MeV O^+ are 1.95 μm and 1.86 μm, and the straggling 0.07 μm and 0.05 μm, respectively. The C-implanted samples were annealed in vacuum to graphitize the damaged layers, and then annealed in air or flowing oxygen. Some samples were etched in a chromic-sulphuric acid solution. The O-implanted samples were annealed in vacuum at 500 - 900°C to form CO_x in the damaged layer, and in some cases a further anneal in O_2 was used to complete the lift-off process. The samples were examined by both optical and scanning electron microscopy to monitor the etching.

C-implanted samples

One set of samples was implanted with 4 MeV C^+ ions to a fluence of $6 \cdot 10^{16}$ cm^{-2}, with the substrate at a temperature of approximately 80K. These samples were annealed in a vacuum of approximately 10^{-6} Torr for 30 min at 950°C to graphitize the buried damaged layers, and then annealed at successively higher temperatures in air to selectively etch the graphitized layers. A sample that was annealed for 2 h in air at 550°C (Fig. 1) showed undercutting of the diamond surface layer by about 9-13 μm from the edges, as demonstrated by interference fringes caused by an air gap between the partially under-cut surface layer and the substrate. One broken-off piece of the surface layer is visible in the figure. The etching rate at 550°C was ~ 5-10 μm/h for the first 4 h. After ~ 20 μm had been undercut, the rate decreased markedly with time. Presumably the etch rate was limited by the penetration of the O in from the edge, and/or by removal of the reaction products CO_x out of the constricted layer. The etching rate at 600°C was higher than at 550°C, but the diamond overlayer was also slowly etched at that temperature. The etching rate of the graphitic layer was about 100 times faster than that of the diamond overlayer. Thus in order to completely etch away the graphitic layer for a 2x2 mm sized crystal, a thickness of about 0.01 mm (10μm) diamond would be removed. Consequently, for this C implantation dose it would be

necessary to protect the diamond overlayer, perhaps by depositing homoepitaxial diamond followed by a diffusion barrier.

After the 950°C vacuum anneal, one of these samples was etched in hot chromic-sulphuric acid, which also caused undercutting by removal of the graphitic layer. A 5 min. etch gave an undercut depth of 0.35 μm, and the overlying natural diamond layer was 2 μm thick.

A second set of samples was implanted with 4 MeV C^+ ions to a fluence of $1 \cdot 10^{18}$ cm^{-2}, also with the substrate at 80K. These samples were annealed in flowing oxygen at 550°C for 1 h. This annealing produced a partially under-cut surface layer, again shown by interference fringes. This sample was then annealed at 550°C for 4 more hours in flowing oxygen. The diamond overlayer had separated when the sample was removed from the furnace, demonstrating that complete lift off required less than five hours at 550°C in flowing oxygen. Both the lifted-off plate and the diamond substrate are shown in Fig. 2. The lifted plate (on the right) is darker than the diamond substrate (on the left). Since darker coloring indicates more irradiation defects, this effect demonstrates that the maximum depth of ion implantation has a sharp cut-off; hence the diamond crystal template has less damage. The line near the edge of both the lifted-off layer and the substrate corresponds to the etching depth after the first hour (about 120μm). The black areas on both the lifted plate and the substrate are unetched graphite.The etching rate at 550°C was determined to be between 120 μm and 140 μm/h, which is much greater than that for the lower dose C-implanted sample described previously.

O-implanted samples

Several samples were implanted at ~80K with 5 MeV ^{16}O ions to fluences of 10^{17} to 10^{18} cm^{-2}. The highest dose was chosen to give a peak oxygen concentration equal to the concentration of host C atoms in the graphitic layer. One of the 10^{18} cm^{-2} samples was annealed at 950°C for 1 h in vacuum. Most of the diamond overlayer flaked off the surface (Fig. 3), presumably because of the high pressure from the reaction products CO and CO_2 at high temperature . A unique mesa structure resulted, as shown in Fig 3a, where well-defined cleavage plane traces are visible. A scanning electron micrograph of one of the remaining pieces on the surface is shown in Fig. 3b. Here residual graphitic layers are visible both on the sample surface and on the underside of the undercut diamond layer. One method by which this unwanted graphite can be removed is by annealing in flowing oxygen.

A second 4x4 mm diamond sample that had been implanted to 10^{18} O ions/cm^2 was etched in flowing oxygen at 550°C for 1 h. Most of the 4x4 mm layer of diamond was removed in one piece, but it broke into 3 pieces while being handled. One of the pieces (4x1.5 mm) was then annealed in vacuum (10^{-5} Torr) at 950°C for 1 h to remove the residual damage. This annealing increased the transparency of the lifted diamond, leaving it curled with a translucent brownish hue, as shown in the SEM micrograph (Fig. 4).

To determine the minimum dose of oxygen needed to lift off a diamond layer, single crystals were implanted with 5 MeV $^{16}O^{+}$ to fluences of $1 \cdot 10^{17}$, $3 \cdot 10^{17}$, and $7 \cdot 10^{17}$ cm^{-2} at 80 K. A dose of $1 \cdot 10^{17}$ cm^{-2} was not sufficient to amorphize the diamond or to cause lift-off. However, successful lift-off was achieved for a dose of $3 \cdot 10^{17}$ cm^{-2}. The sample was annealed in flowing oxygen for 4 h at 550° C. The top layer, which lifted off in one piece, was darker than the diamond substrate, as in Fig. 2. Once again, the central part of the lifted layer appeared black, because of unburnt residual graphite. The $3 \cdot 10^{17}$ cm^{-2} fluence should produce a Frenkel defect concentration of ~10 % in the near-surface layer[7], which is close to the damage concentration that is completely recoverable, according to our earlier annealing results[4]. To avoid the curling of the lifted diamond layer, it would be necessary to deposit a thick (~10 μm) homoepitaxial layer before the lift-off in order to endow the top layer with greater mechanical strength.

We have demonstrated that square millimeter-sized areas of diamond can be lifted off intact from natural diamond crystals through a technique combining implantation and selective etching. Both 4 MeV C implantation, followed by selective etching in oxygen or in chromic acid, and 5 MeV O implantation, followed by vacuum annealing and/or annealing in O, were used. Sheets up to 4x4 mm in size were lifted off by the O implantation method.

The authors acknowledge the technical assistance of Dale Hensley, and support from SDIO funds administered by ONR (contract No. N00014-92-C-0081). Research at the Oak Ridge National Laboratory was sponsored by the Division of Materials Science, U.S. Dept. of Energy, under contract DE-AC05-840R21400 with Martin Marietta Energy Systems, Inc.

1. R.W. Pryor, M.W. Geis, and H.R. Clark, Mat. Res. Soc. Symp. Proc. **242** (1992): to be published (Symp. G, Boston, 1991).
2. J.D. Hunn and N.R. Parikh, unpublished research (patent disclosure, 1992).
3. G. Braunstein, A. Talmi, R. Kalish, T. Bernstein and R. Beserman, Radiat. Eff. **48**, 138 (1980).
4. J.D. Hunn, M.L. Swanson, E.A. Hill, N.R. Parikh and G. Hudson, in "New Diamond Science and Technology", eds. R. Messier et al. (MRS, Pittsburgh, 1991) p. 929.
5. E. Yablonovitch, T. Gmitter, J.P. Harbison and R. Bhat, Appl. Phys. Lett. **51**, 2222 (1987)
6. G.S. Sandhu, B. Liu, N.R. Parikh , J.D. Hunn, M.L. Swanson, Th. Wichert, M. Deicher, H. Skudlik, W.N. Lennard, and I.V. Mitchell, Mat. Res. Soc. Symp. Proc. **162**, 189 (1990).
7. J.F. Ziegler, "Transport of Ions in Matter" (TRIM), IBM Corp. software (1991).

Fig. 1. Optical micrograph of a diamond crystal after implantation with 4 MeV C ions to a fluence of $6 \cdot 10^{16}$ cm^{-2}, and subsequent annealing for 0.5 h at 950°C in vacuum, and for 2 h in air at 550°C. Undercutting of about 11μm from the edge is shown by the interference fringes.

Fig. 2. Optical micrograph of lifted-off diamond layer (on the right) beside the original diamond crystal template (on the left). This lift-off was achieved by an implantation of 4 MeV C ions to a fluence of $1 \cdot 10^{18}$ cm^{-2}, followed by an anneal at 550°C for 5 h in flowing oxygen.

Fig 3. (a.) Optical micrograph of a diamond crystal after implantation with 5 MeV O ions to a fluence of 10^{18} cm^{-2}, followed by annealing at 950°C for 1 h in vacuum. Most of the overlayer was lost, but a few rectangular-shaped pieces of the overlayer remained, and are seen as bright areas in the photograph.

(b.) Scanning electron micrograph of one edge of a piece of diamond overlayer from the sample of Fig. 3(a.). The thickness of the layer was 2 μm.

Fig. 4 Scanning Electron Micrograph of a lifted-off diamond layer. The lift-off was achieved by implantation with 5 MeV O ions to a fluence of 10^{18} cm^{-2}, followed by annealing in flowing oxygen at 550°C for 1 h The sample was then vacuum annealed at 950°C for 1 h to remove radiation damage.

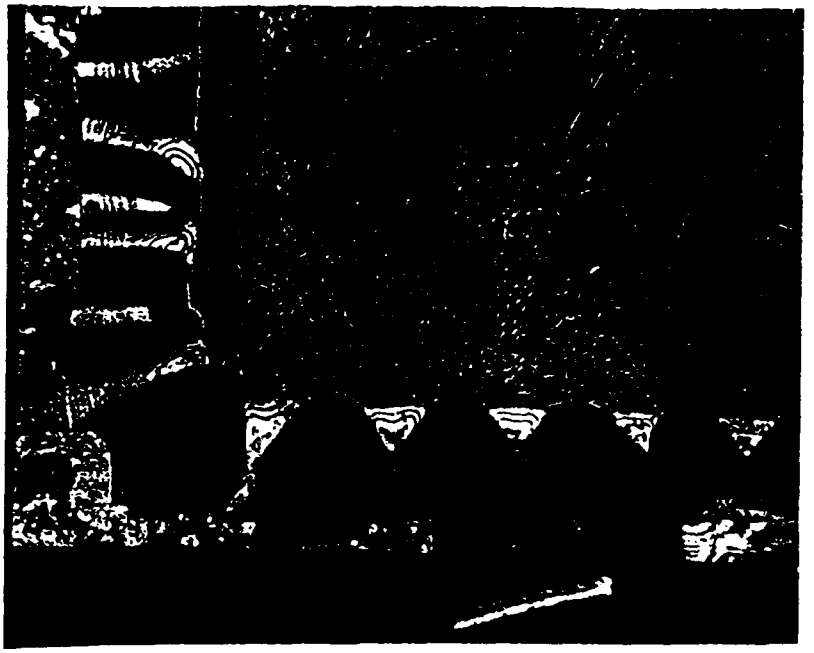

0.5 mm

Fig. 1

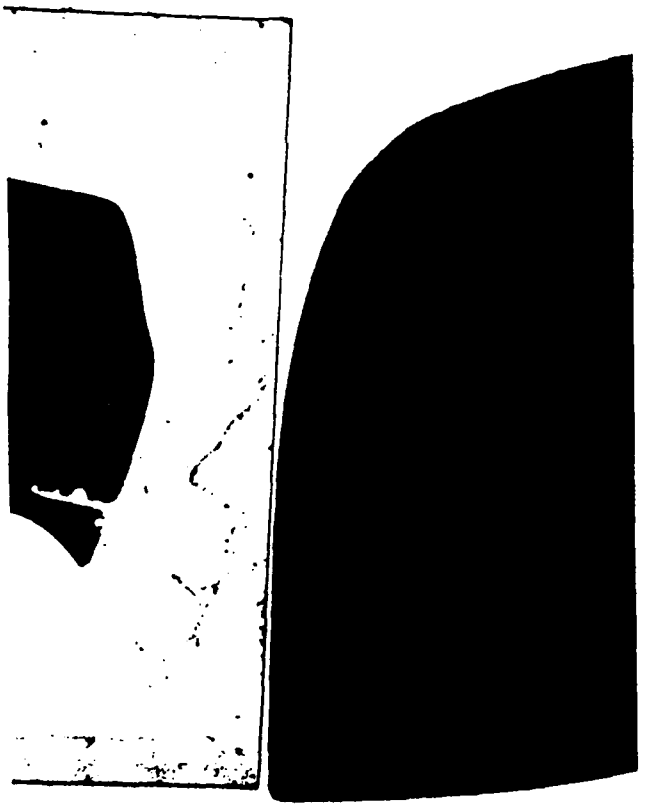

0.5 mm

Fig. 2

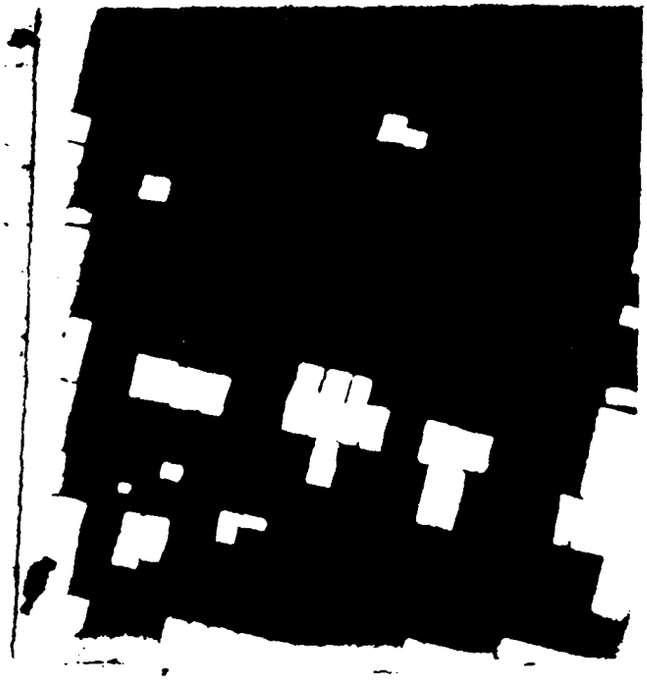

0.5 mm

Fig. 3 a

3.0 μm

Fig. 3 b

0.5 mm

Fig. 4

Formation of diamond films from low pressure radio frequency induction discharges

R. A. Rudder, G. C. Hudson, R. C. Hendry, R. E. Thomas, J. B. Posthill and R. J. Markunas
Research Triangle Institute, Research Triangle Park, NC 27709-2194 (USA)

Abstract

Diamond films have been deposited in a low pressure, radio frequency (r.f.) induction plasma-assisted chemical vapor deposition system. The r.f.-induction system confines the plasma at the low pressures of operation 0.010–10.00 Torr to permit efficient dissociation of the reactant gases. A variety of chemical systems have been used to deposit diamond, including traditional H_2–CH_4 discharges containing 0.5–2.0% CH_4; H_2–CF_4 discharges containing 4–16% CF_4, and water vapor discharges containing high concentrations of alcohol and/or acetic acid vapors. No molecular hydrogen is admitted to the growth chamber for the water-based processes. The water vapor becomes the functional equivalent of the molecular hydrogen used in more traditional H_2–CH_4 discharges. The success of the low pressure r.f.-induction plasma for diamond growth from the wide variety of chemical systems is predicated on the generation of a high electron density plasma. Parent gaseous molecules are converted into appropriate high temperature stable products such as H, H_2, CO, and C_2H_2 as they traverse the plasma. Quadrupole mass spectroscopy has been used to study the conversion of the water–alcohol vapors to H_2, CO, and C_2H_2 as they pass through the r.f. plasma. 99% of the CH_4O is converted into H_2, H_2O, and C_2H_2. These studies show plasma conversion of H_2O into molecular H_2. The excess oxygen is rapidly converted into CO through interactions of the O, presumably with solid carbon sources. Optical emission from both the water-based discharges and the molecular hydrogen-based discharges shows the propensity for atomic hydrogen generation from these low pressure r.f.-induction discharges.

1. Introduction

Diamond film production via chemical vapor deposition has clearly been demonstrated by a vast number of chemical vapor deposition (CVD) techniques [1–10]. Typically, the ability to produce diamond via those CVD techniques depends critically on the production of atomic hydrogen through interaction of molecular hydrogen with hot filaments, microwave plasmas, d.c. arc discharges, or atmospheric r.f. plasma jets. Alternatively, oxy-acetylene torches have been used for the growth of diamond wherein the hot flame provides atomization of gases [6, 7]. We previously reported on the use of a low pressure (less than 10 Torr) r.f.-induction plasma technique for the growth of diamond films from many different feed-stock gases ranging from traditional H_2–CH_4 discharges [11–15], to halogenated H_2–CF_4 discharges [16, 17], to H_2O–alcohol discharges [18], and to H_2O–alcohol–acetic acid discharges [19]. Diamond growth from these varied systems can be associated with the efficient production of atomic hydrogen in the low pressure r.f.-induction discharges.

This paper briefly reviews conditions upon which diamond growth proceeds from the various gas mixtures and then concentrates on analysis and characterization of the water–methanol system for diamond growth. This system is the simplest of the water-based systems and yields great insight into the plasma chemistry. The water-based system may also be of greatest interest to those concerned with commercialization of diamond films. As compared to more traditional growth processes involving H_2–CH_4, the water-based processes offer numerous advantages. Those advantages include: low temperature growth; low pressure operation; the availability of large r.f. power supplies; the elimination of explosive gases from the growth process; the elimination of compressed gases from the growth process.

2. Experimental equipment and procedures

A description of the chemical vapor deposition system used in this work has been previously reported [11–13]. A schematic diagram of the system is shown in Fig. 1. The system consists of a 50 mm ID plasma tube attached to a standard six-way cross. The plasma tube contains an integral water jacket to dissipate heat from the interior quartz wall. An r.f. (13.56 MHz) induction coil couples power from the r.f. power supply into the plasma discharge. Samples are located on a graphite carrier located immediately underneath the induction coil. Samples are heated indirectly by induction heating of the graphite susceptor. If higher temperatures are desired, a supplemental resistive graphite heater can be

0257-8972/92/$5.00

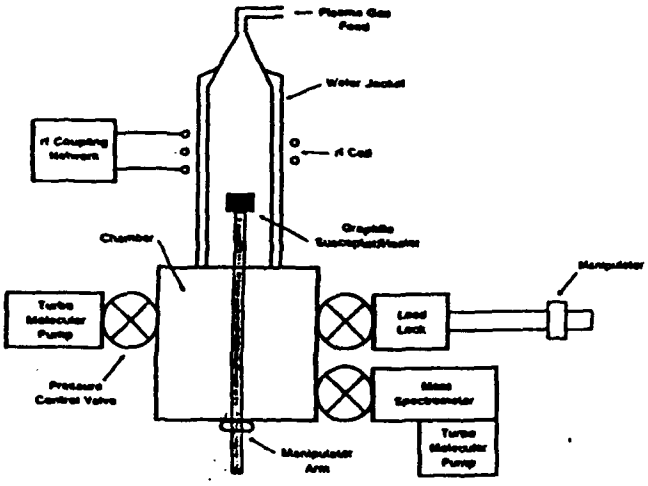

Fig. 1. Schematic of low pressure r.f.-induction plasma-assisted CVD system.

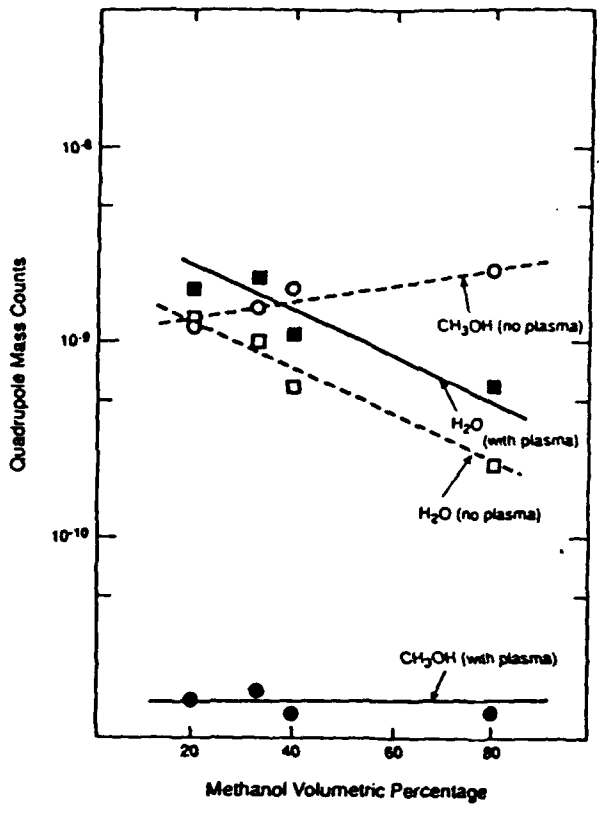

Fig. 2. A plot of H_3O^+ and CH_3O^+ ion counts with and without the r.f.-inductive plasma as a function of the methanol concentration in the liquid reservoir.

used. Care is taken not to insert the graphite carrier into the plasma coil. Insertion into the coil would result in much greater heating of the graphite susceptor.

Gases from compressed sources are introduced into the plasma system through a gas feed at the top of the plasma tube. The gas ratio is controlled by adjusting the relative mass flow rates of each component. Gases above liquid reservoirs (water, alcohol, acetic acid) are introduced into the chamber through a leak valve on a storage tank which contains solutions of the water–alcohol or water–acetic acid–alcohol. Gases from the liquid reservoirs have been introduced either from the top of the plasma tube or at the base of the plasma tube. Either point of introduction can result in diamond growth for an appropriate water to alcohol ratio. In this work, the water to alcohol ratio is dictated by the volumetric ratio in the gas phase above the liquid. Later, in discussing the conversion of the water and alcohol into other gaseous products upon passage through the r.f. discharge, exact ratios of water-to-alcohol in the gas phase are given for the volumetric mixture in the liquid reservoir (see Fig. 2). The practice of mixing the solutions into one storage tank allows a convenient method for evaluating different ratios of water-to-alcohol without the necessity of a gas manifold. There will be some depletion from the solution of the higher vapor pressure component. For the experiments performed here, the liquid loss rate is only 0.2 cm^3 h^{-1}. Accordingly, for relatively short growths (under 10 h) only about 2 cm^3 is lost from a total volume of about 100 cm^3. In a worse case, the depletion of the higher vapor pressure component would only represent a 2% change.

Samples are introduced to the growth system through a vacuum load lock. Prior to insertion, samples were subjected to a diamond abrasive treatment with 1 μm diamond paste to enhance nucleation. Diamond growth proceeds by initiating a r.f.-induction plasma with sufficient power to create intense atomic hydrogen emission. For each gas combination and pressure, there exists a critical power at which the discharge suddenly becomes locally very intense within the r.f. coils. The authors believe that this power threshold is a consequence of the power coupling changing from E-field coupling at low powers to B-field coupling at high powers. Amorim *et al.* [20] have shown in low pressure Ar plasmas that the coupling changes from capacitive coupling to induction coupling at a critical power level depending on the Ar pressure. For Ar at 130 mTorr, the critical power is *ca.* 275 W. The B-field coupling is characterized by intense plasma luminosity from a region of high electron density, *ca.* 10^{12} cm^{-3}. The E-field coupling at lower powers is characterized by weak plasma luminosity from a region of low electron density, *ca.* 10^{10} cm^{-3}. Establishing the high electron density plasma is critical in order to produce diamond growth in this low pressure r.f.-induction system. Attempts to deposit diamond under low density plasma conditions with concentrations of CH_4 in H_2 used for diamond deposition under high power conditions were unsuccessful in producing any film growth, diamond or non-diamond.

This work concentrates on understanding the necessity

of the high electron density plasma for diamond growth by examining the plasma chemistry through optical emission and quadrupole mass spectroscopy. Optical emission spectroscopy has determined the proficiency of the process to produce atomic hydrogen. Quadrupole mass spectroscopy (performed through differential sampling of the gases at the base of the reactor tube) has determined reaction products formed as the parent gases traverse the high-temperature plasma region. Following diamond deposition, samples were analyzed using scanning electron microscopy (SEM) and Raman spectroscopy to ascertain the quality of diamond growth.

3. Experimental results and discussion

Previous work [11–19] has demonstrated the diversity of the low pressure r.f.-plasma technique for the growth of diamond films from a variety of chemical systems under vastly different input powers, substrate temperatures, and pressure conditions. Fig. 3 depicts diamond growth from three different chemical systems ($H_2:CH_4$, $H_2O:CH_4O$, and $H_2O:CH_3COOH:CH_4O$). Table 1 shows experimental differences between the conditions used to deposit diamond in Figs. 3(a)–3(c). Despite the vast differences in deposition conditions, well faceted diamond growth occurs under all these conditions even at low temperatures and low input power. In addition, the low temperature growth capability now permits diamond growth studies on relatively low-melting-temperature materials such as Al.

Critical to the diamond growth in all these processes is the establishment of a high density plasma. While the amount of power necessary to achieve a high density varies from one gas mixture to another, in general, lower pressure discharges require less power to achieve induction coupling. Figure 4 is a plot of the critical power necessary to achieve a high density plasma for the

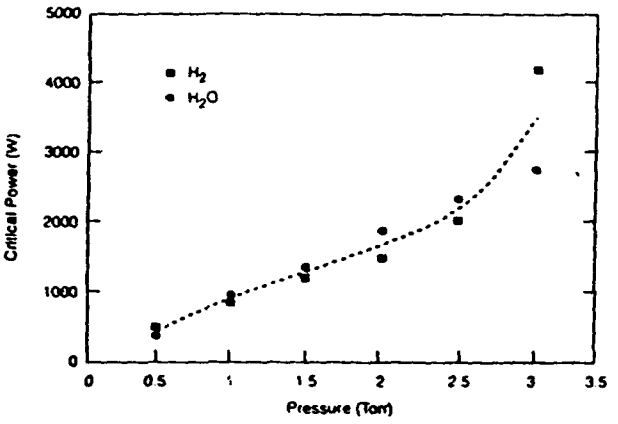

Fig. 4. A plot of critical power necessary to achieve a high density plasma for both H_2 and $H_2O:CH_4O$ mixtures as a function of pressure.

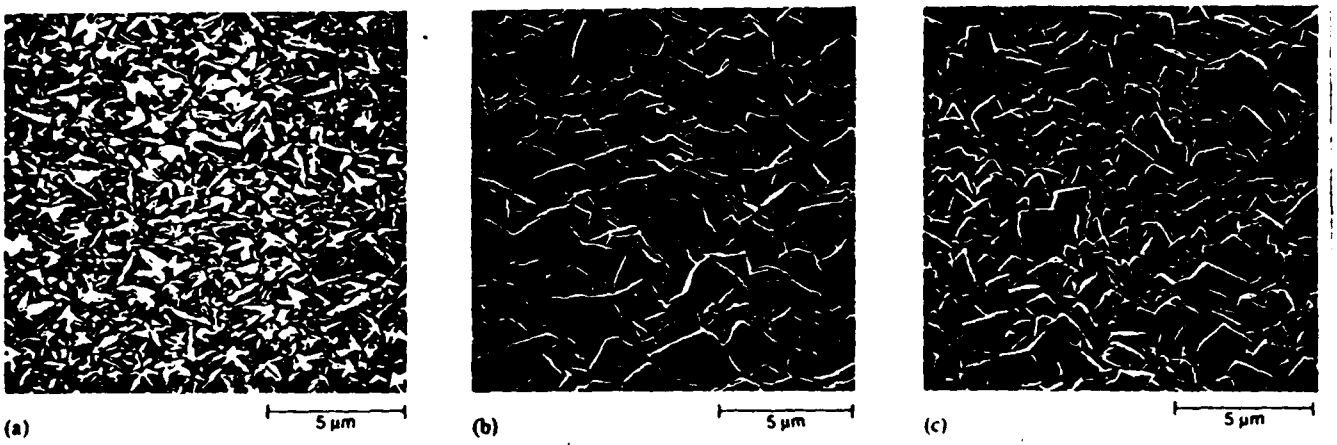

Fig. 3. Scanning electron micrographs from various polycrystalline diamond films deposited from: (a) CH_4 in H_2 on Si(100); (b) CH_4O in H_2O on fused silica; (c) CH_4O in H_2O and CH_3COOH on an aluminium alloy BC 23.

TABLE 1. Deposition conditions for diamond shown in Figure 3

Sample	Figure	Pressure (Torr)	R.f. power (W)	Substrate	t_s (°C)	Gas	Mixture	Deposition rate (μm h^{-1})
1	(a)	5.0	2000	Si	800	$H_2:CH_4$	99:1	1
2	(b)	1.0	1000	Fused silica	300	$H_2O:CH_4O$	2:1*	0.8
3	(c)	0.5	800	Al	300	$H_2O:C_2H_4O_2:CH_4O$	2:2:1*	0.4

*These are the volumetric ratios of the constituents in solution.

H_2:CH_4 and H_2O:CH_4O systems as a function of pressure. The threshold power necessary to establish the high density plasma varies almost linearly with pressure (in this pressure range) for the H_2O:CH_4O system. The H_2:CH_4 system behaves supralinearly so that at higher pressures there is a significant power difference between operating a water-based process and operating a molecular-hydrogen-based process.

3.1. Optical emission

Optical emission spectroscopy was used to confirm atomic hydrogen generation from these low pressure discharges. Figure 5 shows the optical emission from a 3 Torr 1% CH_4 in H_2 discharge. The emission is dominated by the 656 nm atomic hydrogen emission from the transition from the $n=3$ to the $n=2$ energy level. Correspondingly, the discharge has a characteristic red color. High plasma density water discharges, also show a characteristic red color with emission dominated by the 656 nm atomic hydrogen emission. Addition of CH_4O to the high density water discharges results in a bluish-red emission still with dominant atomic hydrogen emission. Figure 6 shows an optical emission spectrum from a 1 Torr H_2O:CH_4O discharge containing approximately equal parts H_2O and CH_4O in the gas phase. Like the diamond producing 1% CH_4 in H_2 discharge, emissions from the water-methanol show intense atomic hydrogen emission even with high CH_4O concentrations. In contrast, low plasma density water discharges are bluish in color with the dominant emission from OH bands and very little atomic hydrogen emission.

3.2. Quadrupole mass spectroscopy

Quadrupole mass spectroscopy has been used to monitor the conversion of parent H_2O, CH_4O molecules

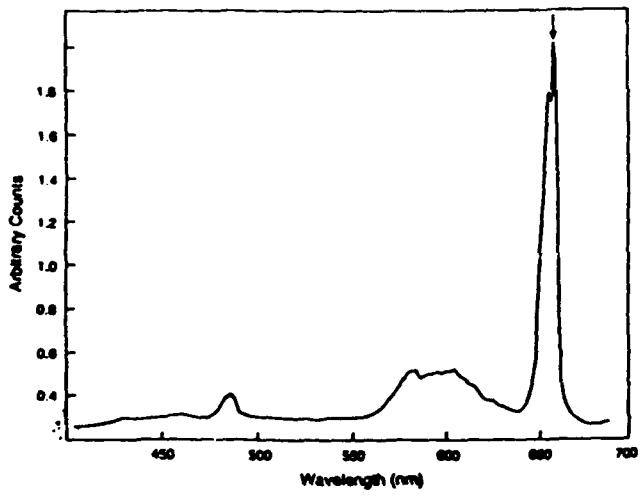

Fig. 5. Optical emission spectrum from at 1% CH_4 in H_2 r.f.-inductive discharge at 3.0 Torr.

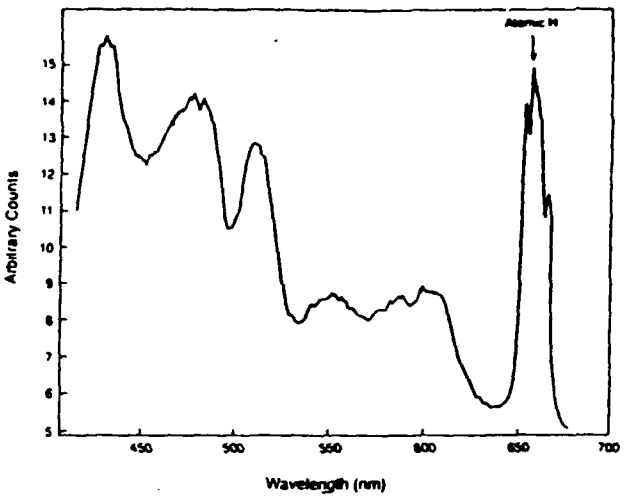

Fig. 6. Optical emission spectrum from a H_2O:CH_4O (1:1) r.f.-inductive discharge at 1.0 Torr.

to high-temperature-stable products as they traverse the plasma. Figure 2 shows H_2O^+ and CH_3O^+ ion counts before and after initiation of the high density plasma. Figure 2 also shows those ion counts as a function of the volumetric concentration of methanol in the liquid reservoir. Before initiation of the plasma, the ratio of H_2O^+ and CH_3O^+ ion counts reflect Raoult's Law relating the partial pressures above a solution to the vapor pressure of the constituent multiplied by its mole fraction in solution. However, after plasma initiation, a rather dramatic occurrence is observed. Nearly all the CH_4O is converted upon traversing the plasma. The CH_3O^+ counts after plasma initiation are only a couple of percent of the original CH_3O^+ counts. Even more knowledge of the plasma dissociation is obtained when one examines by-products from the H_2O:CH_4O plasma discharge. Figure 7 shows the dominant conversion products observed as a function of methanol concentration in the reservoir. A high fraction of molecular H_2 is produced in the gas phase almost regardless of the CH_4O concentration. Molecular H_2 is the dominant species produced by the H_2O:CH_4O plasma discharge. CO and C_2H_2 are also produced as a by-product of the H_2O:CH_4O plasma discharge. At high water concentrations (*i.e.* high oxygen fraction), CO is the preferred gaseous carbon product. At high CH_4O concentrations (*i.e.* low oxygen fraction), C_2H_2 is the preferred gaseous carbon product. Thus, we have identified H_2, CO, and C_2H_2 as conversion products in the high density water–methanol plasma discharges. The water concentrations in the discharge remain high, but the CH_4O concentrations are reduced to only a small percentage of their original concentrations. The production of CO and C_2H_2 can occur via direct conversion of CH_4O into CO or C_2H_2 or via gasification of solid carbon through interactions of oxygen and hydrogen with graphite.

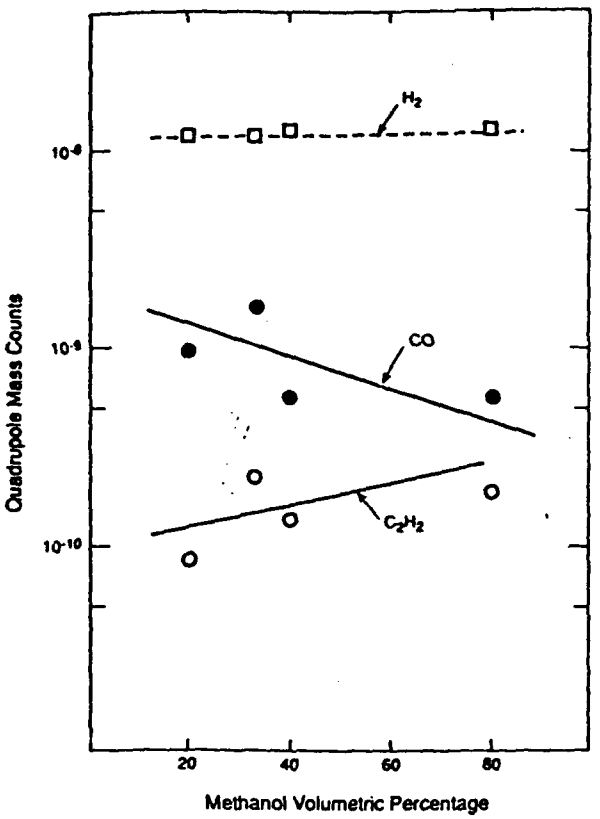

Fig. 7. A plot of the dominant by-products observed from the r.f.-inductive plasma as a function of the methanol concentration in the liquid reservoir.

It is abundantly clear that the water-based processes convert parent H_2O and CH_4O molecules into more stable high temperature products. One can estimate an effective temperature of the plasma by comparing the H_2O to H_2 conversion in the plasma to that predicted from thermodynamic equilibrium. Lede *et al.* [21] have reported on the direct thermal decomposition of water at elevated temperatures (1500–4000 K) at pressures from 10^4 to 10^6 Pa. At temperatures in excess of 3300 K, H_2O is no longer the dominant species. Atomic hydrogen and atomic oxygen are the dominant species at high temperature. From the quadrupole data in Fig. 7, one can estimate the partial pressure of H_2O in the system with the discharge initiated. By taking into account differences in ionization efficiency and differences in mass conductances of H_2, H_2O, and CO, we estimated the partial pressure of H_2O in the growth chamber with the discharge on to be 0.28 Torr. Compared to the partial pressure of 1 Torr for H_2O in the system before the discharge was initiated, the amount of H_2O dissociated by the plasma is 72%. Referring to the 10^4 Pa data given by Lede *et al.* [21], dissociation of 72% of the water would require a temperature of *ca.* 3100 K for homogeneous dissociation. Thus, the low pressure r.f.-induction technique generates an extremely hot plasma. For comparison at 2300 K, only 4% of the water is decomposed under atmospheric pressure. (This amount is expected to increase some as the pressure is reduced.) One key to the success of the growth of diamond at low pressures is undoubtedly the high generation rate of atomic hydrogen in these r.f.-induction discharges. At low pressures, atomic hydrogen can rapidly diffuse from the plasma discharge and recombine on reactor walls. The diffusion depletes the gas phase of atomic hydrogen. Correspondingly, high generation rates must occur to maintain a high concentration of atomic hydrogen. The high generation rates are insured by the high temperatures of the r.f.-induction plasma.

4. Conclusions

Diamond films have been produced from a great variety of chemical systems in a low pressure r.f.-induction plasma-assisted CVD system. Key to this process is the generation of high density plasmas in which efficient atomic hydrogen is possible. Optical emissions from both the water–methanol and the H_2–CH_4 high density discharges show strong atomic hydrogen emission. Quadrupole mass spectroscopy shows that the H_2O:CH_4O system is converted into high temperature stable products H_2, CO, and C_2H_2. Substantial concentrations (*ca.* 25%) of water remain in the system, but almost all the CH_4O is converted. The production of CO and C_2H_2 can occur via direct conversion of CH_4O into CO or C_2H_2 or via reactions of oxygen and hydrogen with nearby graphite. The ability to sustain a high plasma density discharge at low input powers allows diamond growth from the H_2O:CH_4O system to proceed at reduced pressures where recombination on the reactor walls can deplete atomic hydrogen from the gas phase. Estimates of an effective plasma temperature based on the degree of H_2O dissociation shows the effective temperature to be *ca.* 3100 K. Such temperatures are sufficient for atomic hydrogen generation in these low pressure r.f.-induction discharges.

Acknowledgments

The authors wish to thank the support of this work through the SDIO/IST organization and DARPA via ONR contracts N-00014-86-C-0460 and N-000014-91-C-0177. The authors wish to thank Dr T. P. Humphreys and Dr R. J. Nemanich for Raman support during this work. The authors wish to thank D. P. Malta, S. Ammons, and R. V. Durkee for outstanding technical support of this work at Research Triangle Institute.

References

1 B. Derjaguin and V. Fedoseev, *Russ. Chem. Rev., 39* (1970) 783.
2 B. V. Spitsyn, L. L. Bouilov and B. V. Derjaguin, *J. Cryst. Growth, 52* (1981) 219.
3 S. Matsumoto, Y. Sato, M. Kamo and N. Setaka, *Jpn. J. Appl. Phys., 21* (1982) 183.
4 Y. Hirose and Y. Teresawa, *Jpn. J. Appl. Phys., 25* (1986) L51.
5 M. Kamo, Y. Sato, S. Matsumoto and N. Setaka, *J. Cryst. Growth, 62* (1983) 642.
6 L. M. Hanssen, W. A. Carrington, J. E. Butler and K. A. Snail, *Mater. Lett., 7* (1988) 289.
7 G. Janssen, W. J. P. Van Enckevort, J. J. D. Schaminee, W. Vollenberg, L. J. Giling and M. Seal, *J. Cryst. Growth, 104* (1990) 752.
8 Peter K. Bachmann, Dieter Leers and Hans Lydtin, *Diamond Related Mater., 1* (1991) 1.
9 M. Buck, T. J. Chuang, J. H. Kaufman and H. Seki, *Mater. Res. Soc. Symp. Proc., 162* (1990) 97.
10 R. Beckmann, W. Kulisch, H. J. Frenck and R. Kassing, Applications of Diamond Films and Related Materials, *Mater. Sci. Monograph, 73* (1991) 543.
11 R. A. Rudder, G. C. Hudson, Y. M. LeGrice, M. J. Mantini, J. B. Posthill, R. J. Nemanich and R. J. Markunas, *MRS Extended Abstracts EA19*, (1989) 89.
12 R. A. Rudder, G. C. Hudson, R. C. Hendry, R. E. Thomas, J. B. Posthill and R. J. Markunas, Applications of Diamond Films and Related Materials, *Mater. Sci. Monograph, 73* (1991) 583.
13 R. A. Rudder, G. C. Hudson, J. B. Posthill, R. E. Thomas, R. J. Markunas, R. J. Nemanich, Y. M. LeGrice and T. P. Humphreys, Acetylene Production in a Diamond-Producing Low Pressure r.f.-Plasma-Assisted Chemical Vapor Deposition Environment, *2nd Int. Symp. on Diamond Materials* (held during the 179th Meeting of the Electrochemical Society), 1991, in the press.
14 J. B. Posthill, R. A. Rudder, G. C. Hudson, D. P. Malta, R. E. Thomas, R. J. Markunas, T. P. Humphreys, R. J. Nemanich and D. Black, Substrate Effects and the Growth of Homoepitaxial Diamond(100) Layers Using Low Pressure r.f.-Plasma-Enhanced Chemical Vapor Deposition, *2nd Int. Symp. on Diamond Materials* (held during the 179th Meeting of the Electrochemical Society), 1991, in the press.
15 R. A. Rudder, J. B. Posthill, G. C. Hudson, D. Malta, R. E. Thomas and R. J. Markunas, *New Diamond Science and Technology, 1991 MRS Int. Conf. Proc.*, p. 425–430.
16 R. A. Rudder, G. C. Hudson, J. B. Posthill, R. E. Thomas and R. J. Markunas, *Appl. Phys. Lett., 59* (1991) 791.
17 R. A. Rudder, G. C. Hudson, R. C. Hendry, R. E. Thomas, J. B. Posthill and R. J. Markunas, Applications of Diamond Films and Related Materials, *Mater. Sci. Monograph, 73* (1991) 395.
18 R. A. Rudder, G. C. Hudson, J. B. Posthill, R. E. Thomas, R. C. Hendry, D. P. Malta, R. J. Markunas, T. P. Humphreys and R. J. Nemanich, *Appl. Phys. Lett., 60* (1992) 329.
19 R. A. Rudder, J. B. Posthill, G. C. Hudson, D. P. Malta, R. E. Thomas, R. J. Markunas, T. P. Humphreys and R. J. Nemanich, Proc. on Wide-Band Gap Semiconductors, Fall Meet. MRS 1991, Boston, in the press.
20 J. Amorim, H. S. Maciel and J. P. Sudano, *J. Vac. Sci. Technol. B, 9* (1991) 362.
21 J. Lede, F. Lapicque, J. Villermaux, B. Cales, A. Ounalli, J. F. Baumard and A. M. Anthony, *Int. J. Hydrogen Energy, 7* (1982) 939.

2nd International Symposium on ALE, Raleigh, NC, 1992

HYDROGEN-OXYGEN EXCHANGE REACTIONS ON DIAMOND(100) SURFACES

R.E. Thomas, R.A. Rudder, and R.J. Markunas
Research Triangle Institute
Center for Semiconductor Research
Research Triangle Park
North Carolina, 27709-2194
USA
Telephone 919 541-7302
FAX 919 541-6515

We are studying hydrogen--oxygen interactions on diamond surfaces as part of an atomic layer epitaxy (ALE) growth cycle for heteroepitaxial diamond thin films. An ALE sequence designed to grow column IV materials is expected to be quite different than methods currently used for II-VI and III-V materials in that one cannot rely on alternating chemistries associated with the semiconductor constituents. A strategy based on changing the terminating surface species is currently being pursued.

In spite of numerous diamond growth techniques which have been developed to date, relatively little is known concerning gas/surface interactions and surface processes on single crystal diamond. Hydrogen plays a key role in many of the traditional low-pressure diamond growth techniques. Oxygen has been used to extend the diamond growth regime for H_2—CH_4 processes[1] and, in larger concentrations, for the more recently developed water/alcohol growth process[2]. Using thermal mass desorption, LEED, and Auger electron spectroscopy, we have studied interactions of atomic hydrogen and atomic oxygen with both clean and terminated diamond (100) surfaces. Thermal desorption spectra were first measured from surfaces dosed with either atomic hydrogen or atomic oxygen. Desorption spectra were then taken from surfaces sequentially dosed with atomic hydrogen and atomic oxygen, and finally the reverse sequence, atomic oxygen then atomic hydrogen. Molecular hydrogen is the main desorption product observed from surfaces dosed solely with atomic hydrogen. In contrast, CO is the main desorption product from oxygen terminated surfaces. Thermal desorption results from sequentially dosed surfaces indicate that the atomic oxygen is relatively much more efficient at removing adsorbed hydrogen from the surface than atomic hydrogen is at removing adsorbed oxygen from the surface. In addition the atomic oxygen leaves the diamond surface in a 1x1 surface configuration. Hydrogen, in contrast, leaves the surface in a 2x1 configuration which is thought not to be the preferred surface structure for continued growth.

1). J.A. Mucha, D.L. Flamm, and D.E. Ibbotson, J. Appl. Phys. 55, 2179 (1989).
2). R.A. Rudder, et al., Appl. Phys. Lett. 60, 329 (1992).

DIAMOND 1992

COVERING ALL ASPECTS OF DIAMOND AND RELATED MATERIALS

ABSTRACTS

August 31 - September 4, 1992
Convention Center "Stadthalle" Heidelberg, Germany

SURFACE PROCESSES DURING DIAMOND GROWTH FROM WATER-ALCOHOL VAPOR rf-PLASMA DISCHARGES

R.E. THOMAS*, R.A. RUDDER, G.C. HUDSON, and R.J. MARKUNAS
Research Triangle Institute, P.O. Box 12194, Research Triangle Park, NC (USA)

Water-alcohol based diamond growth processes have recently been developed which utilize far higher concentrations of oxygen in the feedstock than in previous growth chemistries. [1] It is currently not clear what role the oxygen plays in these processes. A two-part approach has been adopted to understand the growth chemistries: growth experiments in an rf reactor and separate UHV experiments to study interactions of likely constituent species such as O_2, O, H, OH with clean diamond surfaces.

We find that good quality diamond can be grown at the relatively low substrate temperature of 350°C. Experiments in the rf reactor have shown that water-vapor discharges were much more efficient than hydrogen discharges at etching graphite. A similar process may occur at the growth surface where products from the water vapor discharge etch away non-diamond carbon. In separate surface chemistry studies, thermal desorption spectroscopy, low energy electron diffraction, and Auger electron spectroscopy were used to study interactions of molecular and atomic oxygen with diamond (100) surfaces. Diamond surfaces exposed to atomic oxygen are seen to convert from the 2x1 to the 1x1 state; in contrast to atomic hydrogen which does not break the surface dimer bond at room temperature exposure.[2] CO is the main desorption product from surfaces dosed with atomic oxygen. A broad desorption feature is observed at ~ 600°C. If the temperature ramp is terminated at ~ 800°C, the surface remains in a 1x1 configuration with little oxygen remaining on the surface. Atomic oxygen appears far more efficient than atomic hydrogen in maintaining the (100) surface in a 1x1 configuration. In addition, we find that atomic oxygen easily displaces hydrogen from the diamond (100) surface.

The studies provide a detailed picture of the behavior of oxygen on the diamond surface and clues to the role oxygen plays in the growth process.

1. R.A Rudder et.al. Appl. Phys. Lett. 60 (1992) 329-331.

2. R.E. Thomas et.al. Jnl. Vac. Sci. & Tech A Jul/Aug (1992) in press.

Prime novelty: detailed surface chemistry studies to understand mechanisms associated with a new growth process.
Keywords : thermal desorption spectroscopy, rf-plasma, water-alcohol discharge.

CO & CO_2 Desorption from Diamond (100)

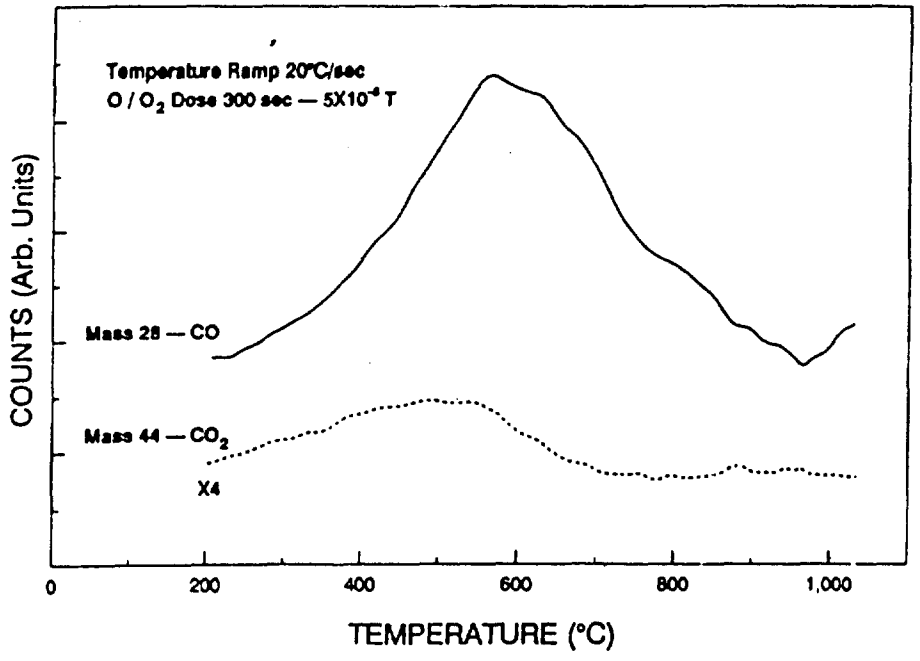

CO Desorption from Oxygen Dosed Diamond (100)

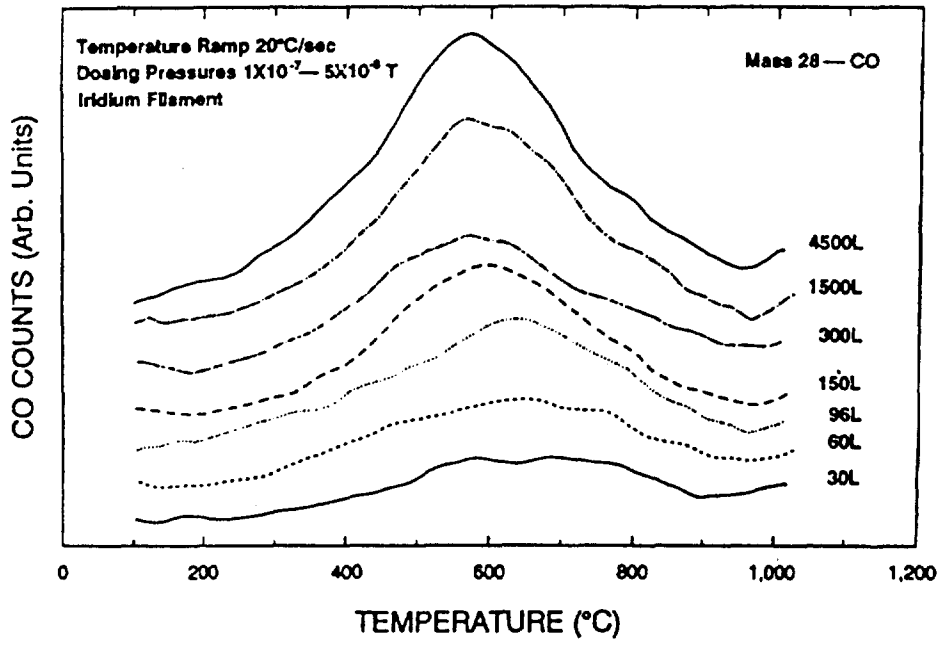

ABSTRACT FORM

INTERNATIONAL CONFERENCE ON METALLURGICAL COATINGS AND THIN FILMS ICMCTF-93

SUBMISSION DEADLINE: 19 OCTOBER, 1992

MANUSCRIPT DUE DATE: 15 MARCH, 1993

Start First Line Here ↓ Underline Title and Speaker's Name Preferred Session Code D2

THE EFFECT OF LOCAL CARBON SOURCES ON DIAMOND NUCLEATION.

R.A. Rudder, G.C. Hudson, J.B. Posthill, and R.J. Markunas, Research Triangle Institute, Research Triangle Park, NC 27709.

Diamond nucleation on non-diamond substrates is an issue that has been widely studied. Many authors have correlated diamond nucleation with advantageous carbon on the wafer surface. However, the chemical constituency and the role of the carbon on the wafer surface have not been rigorously established. We have undertaken nucleation studies wherein a survey of carbon species have been applied to Si wafers without physical abrasion by diamond polish. Experiments were performed in a low pressure rf-induction plasma system using H_2-CH_4 or water-alcohol mixtures. These carbon species have ranged from graphite fibers to fluorocarbon polymers to hydrocarbon polymers to polycarbonates. These experiments suggest that unsaturated carbon species better promote local diamond growth. We suspect that these unsaturated species contribute to diamond nucleation by locally changing the C/H/O ratios nearby the surface without changing the balance of C/H/O in the gas phase region of the plasma. It is critical that the carbon sources upon dissolution not distort the C/H/O ratio in the diamond producing plasma. Independent experiments with higher carbon concentrations in the gas phase do not appreciably enhance diamond nucleation but do degrade the quality of diamond growth.

The author. gratefully acknowledge support of this work by SDIO through ONR (Contract No. N00014-92-C-0081).

Enter session code and number (e.g., A3, F2) from previous pages in upper right hand corner. This should be the session in which you prefer to present your paper.

PROJECTION EQUIPMENT

( ) 35mm Slides

(X) Viewgraphs

( ) Special Equipment (Possible additional cost to the authors) _____

NAME, ADDRESS, FAX NUMBER AND TELEPHONE NUMBER of principal author to receive correspondence:

R.A. Rudder
Center for Semiconductor Research
Research Triangle Institute
Post Office Box 12194
Research Triangle Park, NC 27709

PHONE: 919-541-6765
FAX: 919-541-6515

Names and addresses of three suggested reviewers of the manuscript (Include at least one USA reviewer.)

(1) John C. Angus
Chem. Eng. Dept.
Case Western Reserve Univ.
Cleveland, OH 44106

(2) Pehr Pehrsson
Naval Research Laboratory
Code 6174
Washington, DC 20375

(3) Karl Spear
Penn State
201 Steidle
University Park, PA 16802

MAIL ORIGINAL AND THREE COPIES TO:
ICMCTF-93
Suite 502
1090 G Smallwood Drive
Waldorf, MD 20603 USA
Fax: (301)645-1426

Growth and Characterization of SiGe Contacts on Semiconducting Diamond Substrates

T.P. Humphreys, P.K. Baumann, K.F. Turner and R.J. Nemanich
Department of Physics, North Carolina State University, Raleigh, North Carolina 27695-8202 USA.

K. Das
Kobe Steel Inc., Electronic Materials Center, P. O. Box 13608, Research Triangle Park, North Carolina 27709 USA.

R.G. Alley, D.P. Malta and J.B. Posthill
Research Triangle Institute, Research Triangle Park, North Carolina 27709-2194 USA.

At present, there is a significant scientific and technological interest in the fabrication of stable ohmic and high-temperature rectifying contacts on diamond[1,2]. To date, several metals, [3,4] refractory metal silicides [5] and semiconductors [6] have been investigated as appropriate contact materials to semiconducting diamond substrates. In particular, it has been recently demonstrated by Venkatesan et al.[6] that highly doped polycrystalline p-Si (B doped) and n-Si (As or P doped) contacts fabricated on semiconducting diamond substrates are rectifying at room temperature and at 400 °C. Furthermore, the Si / diamond heterostructure also affords the potential of fabricating novel heterojunction devices which can be integrated with existing Si-based processing technologies.

In this study we report the first results pertaining to the growth and characterization of SiGe contacts deposited on semiconducting natural diamond substrates.

Commercially supplied (D. Drucker & ZN.N.V) low-resitivity (~ 10^4 $\Omega \cdot$ cm, p-type) semiconducting natural diamond (surface orientation (001)) substrates were chemically cleaned. The cleaning procedure included boiling CrO_3+H_2SO_4 (heated to 200°C) for 10 min followed by immersion in aqua regia (3HCl +1HNO_3) and standard RCA cleaning solutions. Following cleaning, the samples were mounted on a Mo sample holder and transferred into the electron-beam evaporation chamber. The base pressure in the system was typically 2 x 10^{-10} Torr. Prior to deposition, the substrates were heated to 550°C for 5 minutes to thermally desorb both water vapor and possibly physi-adsorbed gas contaminants. On cooling to room temperature an unreconstructed (1x1) low energy electron diffraction (LEED) pattern was observed from the C(001) surface. By employing a stainless steel shadow mask several SiGe dots of ~200 nm in thickness and 3 x 10^{-3} cm^2 in area were fabricated. The substrate temperature was maintained at 550 °C during deposition. Corresponding Si and Ge fluxes were calibrated to obtain SiGe layers with a 5% Ge composition.

Examination of the as-grown films by LEED failed to obtain an ordered surface structure. Indeed, an inspection of the SiGe films by *ex-situ* scanning tunneling microscopy (STM) showed a highly textured surface morphology which indicated that the deposited layers were polycrystalline as shown in Fig. 1. The STM image was obtained in the constant current mode with a tip bias of 2 V. The presence of small polycrystalline grains of ~100 nm is clearly evident. The corresponding rms surface roughness of the deposited layer has been determined to be ~ 5 nm.

Raman spectroscopy measurements of the SiGe films obtained at room temperature showed two distinct phonon peaks pertaining to Si and Ge at 518 cm^{-1} and 300 cm^{-1}, respectively. It is interesting to note that the corresponding SiGe phonon mode, indicative of alloy formation (near 400 cm^{-1}) was not observed. The absence of the SiGe phonon mode would tend to suggest an apparent segregation and clustering of Si and Ge during growth. Differences in the Si and Ge surface mobilities and/or surface energies on the chemically cleaned diamond C(001) surface during the initial stages of growth may account for this behavior. Further studies are currently in progress to study this growth phenomena.

Current-voltage (I-V) measurements were obtained by mounting the diamond substrates on a Cu plate using Ag paint to form a large area back contact and applying a bias to the SiGe contact using a W probe. The room temperature I-V characteristics obtained for the SiGe contacts on semiconducting diamond are shown in Fig. 2. The rectifying character of the SiGe film is clearly evident. From the I-V measurements a small forward bias turn-on voltage of ~ 0.6 V was estimated. The corresponding reverse bias leakage current density was measured to be ~1.56 x 10^{-6} A / cm^2 at 20 V. Moreover, from the apparently linear region of the semilogarithmic plot of the forward characteristics an ideality factor n of 2.5 was calculated. This high n value may be an indication that the current conduction at the SiGe/diamond interface is not governed by a thermionic emission mechanism. It is interesting to note that similar observations have also been reported for Ni, $TiSi_2$ and Si contacts on semiconducting diamond C(001) substrates [4,5,6]. In each of these studies current conduction appeared to be dominated by a space charge limited current (SCLC) mechanism. Consistent with the small turn-on voltage and the relatively high reverse leakage current, the corresponding I-V measurements recorded at 400 °C exhibit ohmic-like behavior.

TPH and RJN gratefully acknowledge partial support from the Office or Naval Research (Contract No. N00014-92-J-1477) and Kobe Research Laboratories, USA. TPH, RJN, RGA, DPM, and JBP acknowledge support from the Strategic Defense Initiative Organization / Innovative Science and Technology through the office of Naval Research (Contract No. N00014-92-C-0081).

References

1. M.W. Geis, N.N. Efremow and D.D. Rathman, J.Vac. Sci. Technolol. 6, 1953 (1988).
2. For a review see K.Das, V. Venkatesan, K. Miyata and D.L. Dreifus, Thin Solid Films. 212, 19 (1992).
3. T.P. Humphreys, J.V. LaBrasca, R.J. Nemanich, K.Das and J.B. Posthill, Jpn. J. Appl. Phys. 30, L1409 (1991).
4. K.L. Moazed, J.R. Zeidler and M.J. Taylor, J. Appl. Phys. 68, 2246 (1990).
5. T.P. Humphreys, J.V. LaBrasca, R.J. Nemanich, K.Das and J.B. Posthill, Electron. Lett. 27, 1515 (1991).
6. V. Venkatesan, D.G.Thompson and K. Das, Mater. Res. Soc. 270, 419 (1992).

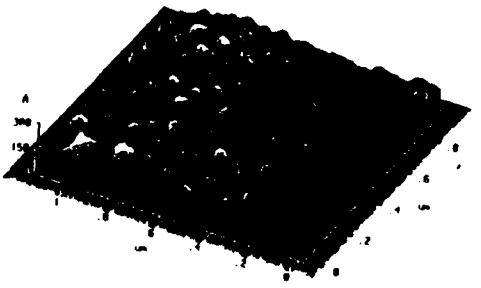

Fig. 1 Topographic (constant current) STM micrograph of the surface morphology of the SiGe film deposited on natural C(001) substrates.

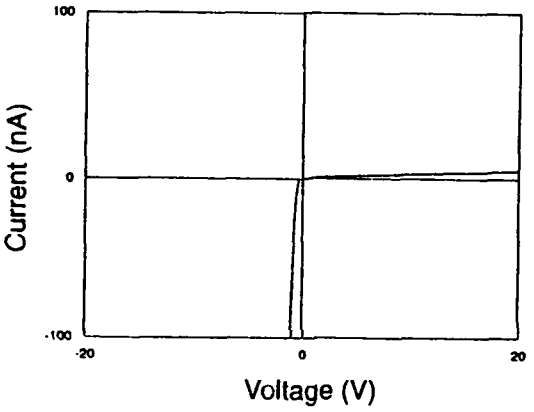

Fig. 2 Linear plot of the current-voltage (I-V) characteristics of the SiGe contacts on semiconducting C(001) substrates. Measurements were conducted at 25°C.

A CORRELATIVE INVESTIGATION OF DEFECTS IN NATURAL AND PECVD-GROWN DIAMOND

D.P. Malta, J.B. Posthill, E.A. Fitzgerald*, R.A. Rudder, G.C. Hudson, and R.J. Markunas
Research Triangle Institute
Research Triangle Park, North Carolina 27709-2194

*AT&T Bell Laboratories, Murray Hill, New Jersey 07974

Many potential electronic applications of diamond require a smooth continuous epitaxial layer with a low defect density. As diamond growth technologies progress toward this goal, focus will shift from the achievement of epitaxial registration to defect reduction in the epitaxial growth. In order to attain defect control, methods of routine and accurate assessment are necessary for an understanding of the nature, origin and propagation of defects in diamond[1].

We have conducted a correlative investigation of structural, electrical, optical, and oxidation properties of defects in natural Type IIb diamond and compared those results to the properties of defects in plasma-enhanced chemical vapor deposition (PECVD)-grown polycrystalline diamond films.

A natural Type IIb semiconducting diamond stone that was cut into three substrates with (100) face orientations was obtained from a commercial vendor. A polycrystalline diamond film was grown on Si(100) by low pressure rf-induction PECVD using an acetic acid/water/methanol mixture at 0.5 Torr and a substrate temperature of 350 °C[2]. Both sample types were investigated using plan-view transmission electron microscopy (TEM), scanning cathodoluminescence (CL), scanning electron microscopy (SEM), electron beam-induced current (EBIC) and a newly developed oxidation/etching method for defect delineation. The natural diamond substrates were cut 100μm thick to minimize ion milling time during TEM sample preparation. The oxidation technique consisted of immersion of the diamond in an oxidizing flame for 3-4 seconds followed by SEM analysis.

Plan-view TEM on (100) Type IIb semiconducting crystals revealed a high ($\sim 10^8 cm^{-2}$) density of dislocations which showed preference for clustering (Fig 1). EBIC and panchromatic CL images indicated that dislocations were arranged in a cellular structure and were electrically active *and* luminescent (Figs. 2a and 2b). Individual dislocations were not resolved due to the small spacing (avg.$\sim$0.5μm) and relatively large electron beam interaction volume diameter ($\sim$4μm at 25KeV). CL collected at 6 °K was strongest

at 430nm, which has been associated with donor-acceptor recombination due to nitrogen and boron impurities[3,4], respectively. Other CL peaks were observed at 589nm, 648nm, and 680nm.

Oxidation/etching of the aforementioned Type IIb diamond crystal formed etch pits at dislocation sites with a density in close agreement with TEM measurements (Fig. 3, compare to Fig. 1). Plan-view TEM of the polycrystalline film (Fig. 4a) revealed a high density of microtwins and possibly dislocations. Due to the very small spacing between these defects, the SEM-based CL and EBIC techniques were incapable of resolving them. Oxidation/etching of a sample grown under the same conditions, however, revealed the twin boundaries (grooves) and dislocations (holes) with high spatial resolution (Fig. 4b).

The flame-exposure process is believed to oxidize diamond forming volatile CO and CO_2 products. Defect sites are presumed to etch faster. Others have reported defect delineation on polycrystalline diamond using furnace annealing[5] and reactive ion etching[6] with oxygen-containing gases. This new method is easy to implement and correlates well with more rigorous techniques such as TEM.

Acknowledgements: The authors gratefully acknowledge the support of this work by the SDIO/IST through ONR (Contract No. N00014-92-C-0081).

References

1. D.P. Malta, S.A. Willard, R.A. Rudder, G.C. Hudson, J.B. Posthill, R.E. Thomas and R.J. Markunas Proceedings of the 49th Annual Meeting of the Electron Microscopy Society of America (Ed. G.W. Bailey, San Francisco Press, 1991) p.880.
2. R.A. Rudder, J.B. Posthill, G.C. Hudson, D.P. Malta, R.E. Thomas, R.J. Markunas, T.P. Humphreys and R.J. Nemanich, Mat. Res. Soc. Symp. Proc., 23 (1992).
3. G. Davies, in: The Properties of Diamond, Ed. J.E. Field (Academic Press, London 1979) Ch. 5.
4. R.J. Graham, J.B. Posthill, R.A. Rudder and R.J. Markunas, Appl. Phys. Lett., 59, 2463 (1991).
5. W. Zhu, X. Hong Wang, A. Badzian and R. Messier, Proceedings of New Diamond Science and Technology, Washington, DC, 812 (1990).

6. Y. Sato, C. Hata, T. Ando and M. Kamo, Proceedings of New Diamond Science and Technology, Washington, DC. 537 (1990).

FIGURE 1: Plan-view TEM of natural Type IIb diamond shows dislocations. Examination of large areas found that dislocations tended to cluster and overall density was $\sim 10^8 cm^{-2}$.

FIGURE 2: Large area maps of defect distributions in natural Type IIb diamond; (a) EBIC image; dark regions represent *all* electron-hole recombination sites, (b) panchromatic CL image; bright regions represent *radiative* electron-hole recombination sites.

FIGURE 3: Oxidation etch pits in natural Type IIb diamond formed at dislocation sites upon exposure to a propane flame in air. Density measured over large areas was $\sim 10^8 cm^{-2}$.

FIGURE 4: Defect images of PECVD-grown polycrystalline diamond; (a) plan-view TEM shows very high density of microtwins and, (b) SEM of similar sample after exposure to propane flame in air identifies microtwin boundaries (grooves) and dislocations (holes).

FIGURE 1: Plan-view TEM of natural Type IIb diamond shows dislocations. Examination of large areas found that dislocations tended to cluster and overall density was $\sim 10^8 cm^{-2}$.

FIGURE 3: Oxidation etch pits in natural Type IIb diamond formed at dislocation sites upon exposure to a propane flame in air. Density measured over large areas was $\sim 10^8 cm^{-2}$.

FIGURE 2: Large area maps of defect distributions in natural Type IIb diamond; (a) EBIC image; dark regions represent *all* electron-hole recombination sites, (b) panchromatic CL image; bright regions represent *radiative* electron-hole recombination sites.

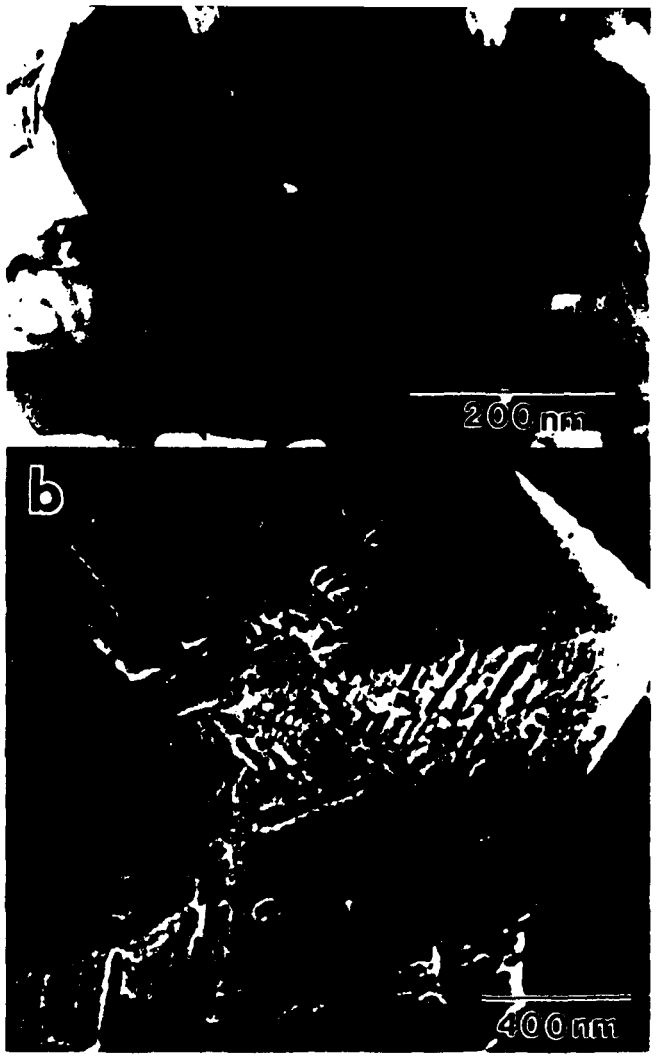

FIGURE 4: Defect images of PECVD-grown polycrystalline diamond; (a) plan-view TEM shows very high density of microtwins and, (b) SEM of similar sample after exposure to propane flame in air identifies microtwin boundaries (grooves) and dislocations (holes).

HOMOEPITAXIAL DIAMOND LAYERS GROWN WITH DIFFERENT GAS MIXTURES IN A RF PLASMA REACTOR

J.B. Posthill, **D.P. Malta**, R.A. Rudder, G.C. Hudson, R.E. Thomas, and R.J. Markunas
Research Triangle Institute
Research Triangle Park, North Carolina 27709-2194

T.P. Humphreys and R.J. Nemanich
Department of Physics, North Carolina State University
Raleigh, North Carolina 27695-8202

The thermal and electrical properties of diamond make it an excellent candidate for electronic applications in extreme environments, but significant device development in this materials system cannot take place unless larger area single crystals are available. While significant progress has been made towards increasing the areal size of diamond crystals by different means[e.g.1,2], it is also recognized that a reliable and inexpensive method of growing high-quality epitaxial diamond will be necessary to grow device structures and to increase the thickness of diamond crystals and films. To this end, we have examined the effect of gas phase chemistry on the homoepitaxial growth of diamond on natural diamond single crystals. A brief outline of some of these results obtained in an rf-driven plasma-enhanced chemical vapor deposition (PECVD) reactor follows.

The substrates used in this study were nominally (100) and (110) oriented [$\pm$ 3°] natural type Ia diamonds. It has been established previously by both X-ray topography and ion channeling studies that type Ia substrates are crystallographically superior[3], and it is believed that this would result in improved diamond homoepitaxial films. Transmission electron microscopy (TEM) of a type Ia diamond showed the expected presence of nitrogen-containing platelets lying on {100}-type planes (Fig. 1). However, no dislocations could be seen in the field of view, hence, the dislocation density is $< 10^5$ cm^{-2}. This contrasts with substantially larger dislocation densities observed in type IIb substrates[4]. Prior to loading into the reactor, substrate preparation involved swabbing in deionized water and blow drying with clean nitrogen. Swabbing has been shown to remove particles from the diamond surface, thereby minimizing the sporadic regions of polycrystallinity that are thought to be caused by this contamination[3].

The system used for the growth of homoepitaxial diamond consists of a 13.56 MHz inductively-coupled plasma-enhanced chemical vapor deposition (PECVD) system. The sample is positioned near the rf coil on a graphite susceptor, and the growth temperature was achieved by a combination of rf inductive coupling to the susceptor and additional heating from an independently driven radiative source beneath the susceptor. A variety of different gas mixtures have been used for diamond growth. In addition to conventional CH_4/H_2 mixtures, we have also explored oxygen-containing mixtures which utilized combinations of CO, CH_4, and H_2. Recently, polycrystalline diamond has been grown using water:alcohol and water:alcohol:organic acid mixtures[5,6]. This new method of CVD diamond growth using inexpensive liquids has been extended to homoepitaxial diamond growth.

Fig. 2 shows an SEM micrograph taken from an epitaxial film grown on a (100) substrate with a 1%CH_4/99%H_2 mixture at a pressure of 5 Torr and temperature of $\sim$ 900 °C. An extensively 'shingled' morphology is evident. Interestingly, micro-Raman spectroscopy taken from the near-surface region of this sample was not found to be severely degraded; the full-width at half-maximum (FWHM) of the diamond LO phonon line at 1332 cm^{-1} was measured to be 2.8 cm^{-1}. Fig. 3 shows a much improved surface topography from an epitaxial film grown on a (110) substrate with a 0.62%CO/0.23%CH_4/99.15%H_2 mixture at P = 5 Torr and T $\simeq$ 900 °C. There are some regions on this sample that exhibit polycrystallinity, which is believed to be due to incomplete particle removal. The micro-Raman shows a FWHM of 2.7 cm^{-1} (Fig. 4). Given that smooth (100) diamond epilayers have been observed previously when grown with comparable $CO/CH_4/H_2$ mixtures[3], it is believed that the presence of the CO is the dominant factor responsible for the superior morphology. However, previous research has shown good (110) diamond epitaxial surface morphologies using only CH_4/H_2 mixtures[7].

Fig. 5 shows the surface of a (100) homoepitaxial film grown by introducing the vapor pressure of a 33.3%CH_3OH/66.7%H_2O liquid mixture at P = 1 Torr and T $\simeq$ 400 °C. The diamond epilayer shows little roughness. Perhaps the most remarkable aspect of this water:methanol diamond film is the measured concentrations for some of the common (and potentially detrimental) elemental impurities. Secondary ion mass spectrometry (SIMS) showed that Si, B, and N were at measured instrumental background, while H and O were measured to be 2×10^{18} cm^{-3} and 3×10^{18} cm^{-3}, respectively. *All* these values are the lowest that we have observed in any of our high-temperature-grown homoepitaxial diamond films. No special distillation/purification was performed to the liquid reagents to achieve this result. It appears that water:alcohol mixtures can be used where a low temperature diamond epitaxial process is desired or required.

Acknowledgements: The authors gratefully acknowledge the support of this work by the SDIO/IST through ONR (Contract No. N00014-92-C-0081).

References

1. M.W. Geis, H.I. Smith, A. Argoitia, J. Angus, G.-H.M. Ma, J.T. Glass, J. Butler, C.J. Robinson, and R. Pryor, Appl. Phys. Lett., 58, 2485 (1991).
2. B.R. Stoner and J.T. Glass, Appl. Phys. Lett., 60, 698 (1992).
3. J.B. Posthill, R.A. Rudder, G.C. Hudson, D.P. Malta, G.G. Fountain, R.E. Thomas, R.J. Markunas, T.P. Humphreys, R.J. Nemanich, and D.R. Black, Proc. of the 2nd Intl. Symp. on Diamond Materials, 91-8, [The Electrochemical Society], 274 (1991).
4. D.P. Malta, J.B. Posthill, E.A. Fitzgerald, R.A. Rudder, G.C. Hudson, and R.J. Markunas, [this proceedings].
5. R.A. Rudder, G.C. Hudson, J.B. Posthill, R.E. Thomas, R.C. Hendry, D.P. Malta, R.J. Markunas, T.P. Humphreys, and R.J. Nemanich, Appl. Phys. Lett., 60, 329 (1992).
6. R.A. Rudder, J.B. Posthill, G.C. Hudson, D.P. Malta, R.E. Thomas, R.J. Markunas, T.P. Humphreys and R.J. Nemanich, Mater. Res. Soc. Symp. Proc., 242, 23 (1992).
7. W.J.P. van Enckevort, G. Janssen, W. Vollenberg, M. Chermin, L.J. Giling, and M. Seal, Surf. and Coating Tech., 47, 39 (1991).

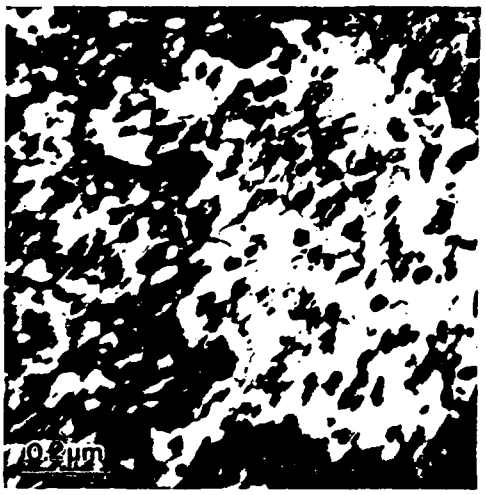

Fig. 1 -- TEM of natural type Ia diamond substrate showing 50nm diameter nitrogen platelets on {100}-type planes. No dislocations were observed.

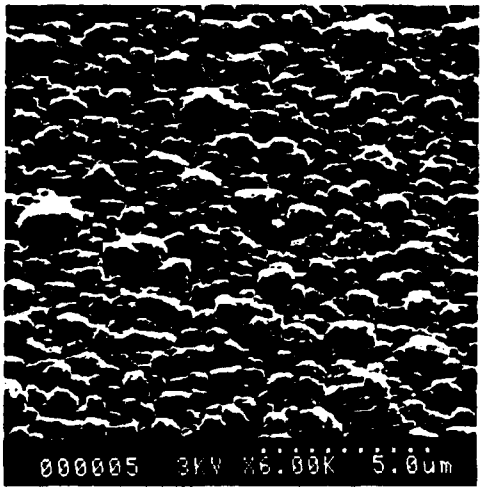

Fig. 2 -- SEM of 1%CH_4/99%H_2 homoepitaxial (100) diamond.

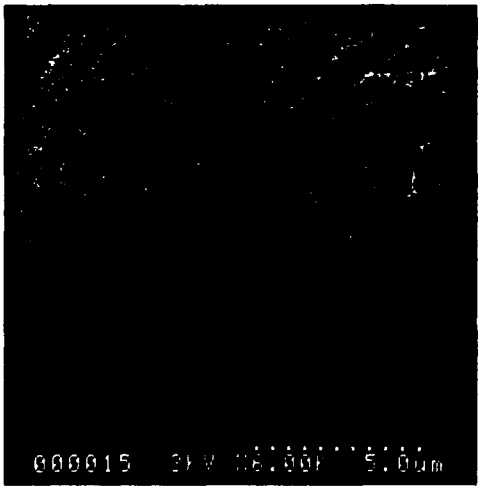

Fig. 3 -- SEM of 0.62%CO/0.23%CH_4/99.15%H_2 (110) homoepitaxial diamond.

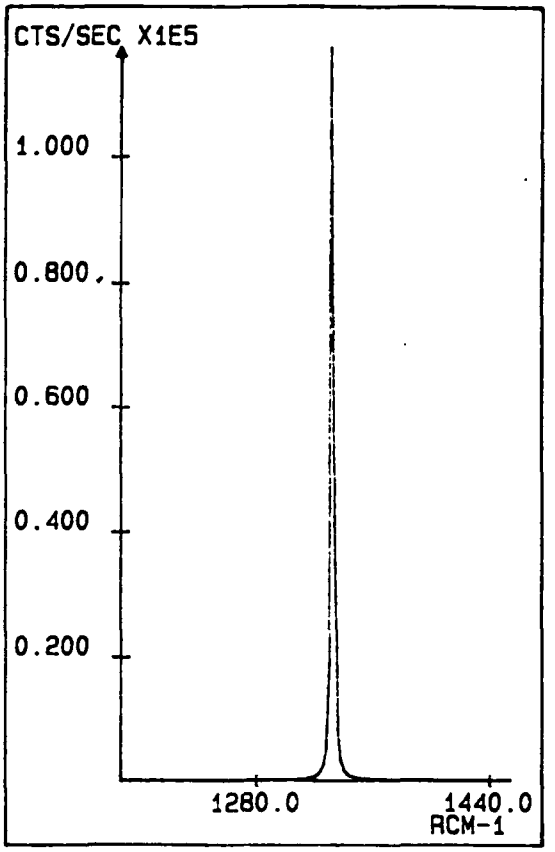

Fig. 4 -- Micro-Raman spectrum from the near-surface of 0.62%CO/0.23%CH_4/99.15%H_2 (110) homoepitaxial diamond.

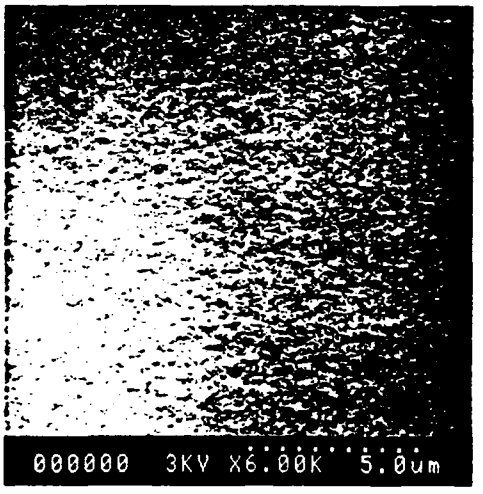

Fig. 5 -- SEM of 33.3%CH_3OH/66.7%H_2O (100) homoepitaxial diamond.

DIAMOND SURFACE STUDIES OF GROWTH MECHANISMS FROM WATER-ALCOHOL DEPOSITION CHEMISTRIES

R.E. Thomas, R.A. Rudder, and R.J. Markunas,

Research Triangle Institute

Research Triangle Park, NC 27709.

Diamond growth chemistries have been developed which rely solely on vapors from water-alcohol mixtures.[1] The relative concentrations of C,O, and H used in the liquids puts the mixtures within the confines of the "Bachmann triangle", towards the hydrogen rich corner of the diagram.[2] Although numerous growth chemistries have utilized oxygen as a key component, the role that oxygen plays is still not well understood. In this paper we will be presenting results from diamond growths using water-alcohol mixtures and results from basic surface chemistry studies of interactions of atomic oxygen with single crystal diamond (100) surfaces.

In general, we find that diamond (100) surfaces are left in a 1x1 configuration following polishing and wet chemical cleans. Auger analysis of samples as introduced to the vacuum chamber reveals oxygen concentrations equivalent to those seen after in vacuo saturation of the surface with atomic oxygen. Although it has long been thought that diamond surfaces were hydrogen terminated following cleaning, results here indicate that oxygen is responsible for producing the 1x1 configuration on the diamond surface. In fact, calculations indicate that it is difficult to produce a saturated dihydride surface on the diamond (100) face.[3] After annealing to approximately 1100°C, LEED observations on these samples indicate the surfaces convert from the 1x1 phase to the 2x1 phase. Dosing of the samples in the 2x1 state with atomic oxygen will then convert them back to the 1x1 configuration. Figure 1 shows possible bonding configurations for oxygen on the diamond (100) surface.

Figure 2 shows a series of thermal desorption spectra from oxygenated diamond (100) surfaces. The main desorption product from oxygen terminated (100) surfaces is CO, with a maximum desorption rate at approximately 600°C. Additional thermal desorption experiments were performed where the heating rate was varied in order to extract activation energies for the desorption of CO and Co_2 from the oxygenated surfaces. Results shown in Figure 3 show thermal desorption spectra for CO as a function of heating rate and the analysis to determine the activation energy. Activation energies of approximately 44 kcal/mole and 21 kcal/mole were found for CO and CO_2 desorption respectively.

If the desorption ramp is continued to approximately 1050°C and the samples are cooled they are found to be in the 2x1 configuration. However, if the temperature ramp is terminated at approximately 650°C, most of the oxygen has desorbed from the surface as CO, but upon cooling the surface is found to remain in the 1x1 configuration. Figure 4 shows hydrogen and CO desorption spectra from a series of thermal desorptions where hydrogen was used to probe the 1x1 sites left open by the CO desorption. Figures 4a and 4e give results from samples exposed only to oxygen and hydrogen respectively for comparison. Figures 4b, 4c, and 4d give results for samples that were saturated with atomic oxygen at 25°C and then exposed to atomic hydrogen at 550°C, 650°C, and 800°C respectively. The samples were cooled, surface structure was determined by LEED, and then thermal desorption spectra were taken. Results from samples exposed to atomic hydrogen at 550°C and 650°C indicate that oxygen remained on the surface after annealing under an atomic hydrogen flux. In addition both samples remained in the 1x1 configuration. In contrast, the sample annealed at 800°C converted from the 1x1 to the 2x1 configuration and it appears that very little oxygen was left on the surface following the anneal. Although Figures 4b and 4c show the hydrogen desorbing from what appears to be 1x1 sites on the surface, the hydrogen desorption spectra appear identical to desorption spectra taken from samples that were dosed with atomic hydrogen while in the 2x1 configuration. In the case of silicon, two desorption peaks are generally observed upon desorption from the dihydride silicon surface. The lower temperature desorption peak from silicon is usually associated reconstruction from 1x1 to the 2x1 configuration and the second peak is from the monohydride phase. To study hydrogen desorption further two separate experiments were performed on a diamond sample. In the first the surface was converted to the 1x1 configuration by saturating with atomic oxygen and partially desorbing the oxygen. A second sample was prepared by completely desorbing oxygen and converting the surface to the 2x1 configuration. Both samples were then dosed with equivalent quantities of atomic hydrogen at 25°C and thermal desorption spectra were taken. Hydrogen desorption peaks from both samples occurred at the same temperature and were very similar in appearance. With regard to hydrogen desorption there does not appear to be a large difference between sites on a nominally 1x1 surface and the 2x1 diamond surface.

The results for oxygen reactions with the diamond surface indicates that atomic oxygen can play many of the roles that have traditionally been attributed to atomic hydrogen. Specifically, atomic oxygen has the ability to both maintain and restore sp^3 bonding on the surface as evidenced by the LEED observations. Atomic oxygen may assist in the removal of non-diamond carbon from the growth surface.[5] Finally, desorption of CO from the surface leaves sites open for addition of carbon to the lattice. Although two carbon atoms need to be added to replace the one removed, the opening of sites can occur at temperatures as low as 250°C, as shown with the thermal desorption results.

Acknowledgements: The authors gratefully acknowledge the support of this work by the SDIO/IST through ONR (Contract No. N00014-92-0081).

1) R.A. Rudder et al., Appl. Phys. Lett., **60**, 329 (1992).

2) P.K. Bachmann, et al., Diamond and Related Materials, **1**, 1 (1991).

3) R.E. Thomas, et al., J. Chem. Vap. Dep. **1**, 6 (1992).

4) R.E. Thomas, et al., J. Vac. Sci. Technol. A **10**, 2451 (1992).

5) P.K. Bachmann, et al., paper 13.16, presented at Diamond 1992, Heidelberg, Germany, 1992.

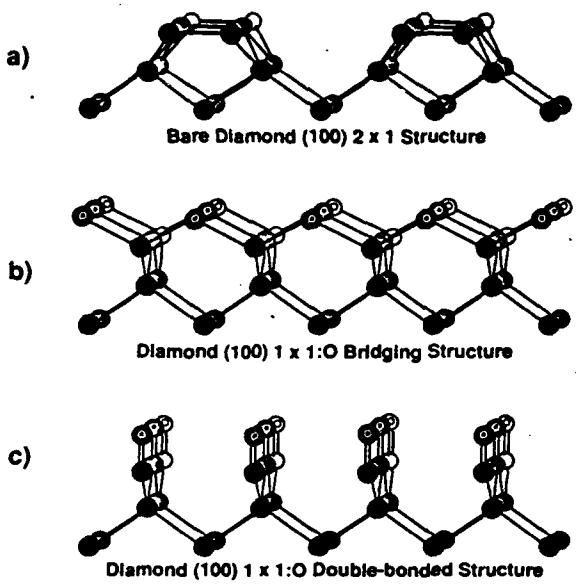

Fig. 1.(a) shows a clean diamond (100) surface in the 2x1 configuration. (b) and (c) show 2 possible bonding configurations which would give a 1x1 LEED pattern.

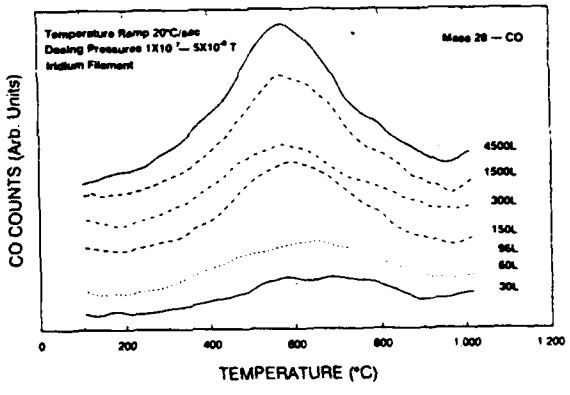

Fig. 2. Thermal desorption spectra from oxygen dosed diamond surfaces. Samples were exposed to a mixture of O and O_2, after molecular oxygen was passed over an iridium filament.

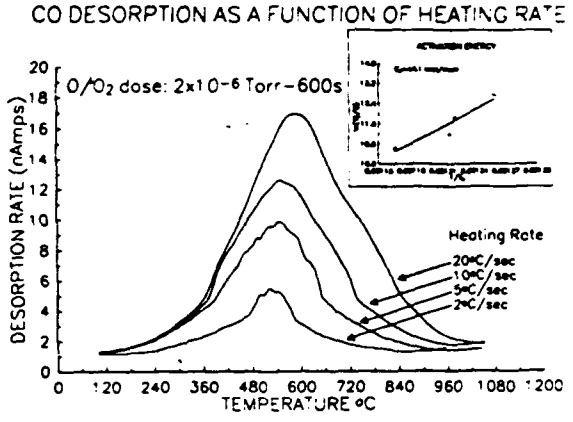

Fig. 3. CO desorption spectra as a function of heating rate. The inset graph shows the extraction of the activation energy for the desorption of CO, approximately 44.1 kcal/mole.

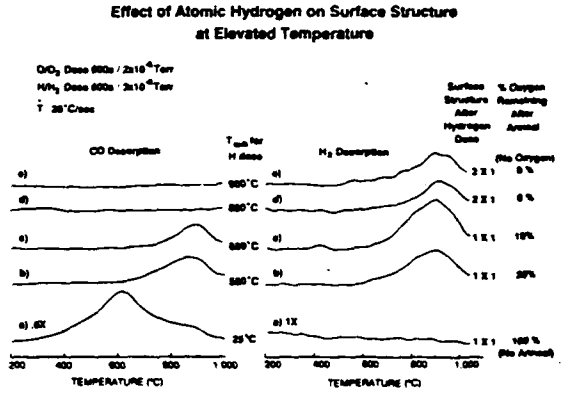

Fig. 4. Thermal desorption spectra from samples which were first dosed with oxygen and then dosed with atomic hydrogen at a series of temperatures around the CO desorption peak of 600°C. LEED patterns from the surface after hydrogen dosing show that we are able to maintain a 1x1 surface structure up to approximately 650 °C, but at higher temperatures the the remaining oxygen is lost and the surface reconstructs to the 2x1 phase.

LOW TEMPERATURE DIAMOND GROWTH: DEVELOPMENT OF WATER-BASED TECHNIQUES FOR DIAMOND CVD

R.A. Rudder, R.E. Thomas, G.C. Hudson, J.B. Posthill, D.P. Malta, and R.J. Markunas

Research Triangle Institute Research Triangle Park, NC 27709.

Recently, we have demonstrated, and others have reproduced chemical vapor diamond deposition from water solutions containing alcohols and organic acids. These techniques have been quite successful in depositing diamond at temperatures well below 600°C. These demonstrations have taken place in low pressure rf induction plasma systems[1,2] and in low pressure microwave ECR systems[3,4]. Diamond deposition at temperatures below 600°C allows for the application of diamond thin films on materials which can not survive high temperature growth. Our work has concentrated on diamond growth from low pressure rf induction plasmas. These plasmas have shown a great propensity for diamond deposition. Diamond growth from low pressure rf induction plasmas occurs when sufficient power is applied to the rf coils to inductively couple to the plasma gas. Diamond growth below this critical power level proceeds very slowly, if at all. This can be understood by considering the plasma density when the power is capacitively coupling verses rf induction coupling. Inductively coupled discharges have about a two-order of magnitude higher plasma density than do capacitively coupled discharges. Along with inducing currents in th plasma gas, the radiation field from the rf coil produces eddy currents in the sample and the sample stage. For low temperature diamond deposition, the applied power needs to be reduced in order to avoid high substrate temperatures.

We have found that diamond growth can be obtained at lower and lower applied powers 1) if the molecular hydrogen is replaced by alternative sources of atomic hydrogen which have lower ionization potentials and 2) if the operating pressure is reduced. Table I shows a list of ionization potentials for those gasses which we have used during diamond growth in the low pressure rf induction system.

Table I. Ionization potentials

H_2	15.4
H_2O	12.6
CH_3OH	10.9
CH_3CH_2OH	10.5
CH_3COOH	10.7

Empirically, we have found that the critical power level necessary to inductively couple and, in turn, the critical power necessary for diamond growth falls as one introduces gasses with lower ionization potentials. Furthermore, we have observed that the critical power level is a strong function of the growth pressure. Figure 1 shows the critical power to inductively couple as a function of pressure for pure water discharges and for pure hydrogen discharges. At low pressure, there is not a pronounced difference. However, at more typical growth pressures (above 1 Torr), the water discharges require considerably less power input.

The water/alcohol discharges require considerably less power than the molecular hydrogen discharges to achieve induction coupling and consequently to grow diamond. Furthermore, the addition of acetic acid to the water solution allows even lower input power to be applied to the rf coil. These innovations now allow diamond growth to proceed at very low temperatures, perhaps as low as 250°C. Figure 2 shows SEM micrographs from a sample deposited from the vapors above a room temperature acetic-acid:water:methanol solution. The input power to the rf coil was $\sim$ 500 W. Under these conditions, a continuous film was not obtained. Discrete diamond particles were produced. The diamond particles grew in a very anisotropic fashion. Micro-Raman from these crystals shows (shown in Figure 3) these crystals to have a very narrow FWHM of 2.9 cm^{-1} with negligible amorphous carbon or graphitic component.

It is certainly encouraging that the material quality did not degrade at the low temperature. This one data point suggests that very high quality diamond can be grown at remarkably low temperatures. Preliminary experiments have been undertaken to determine a low temperature limit to the process by actively cooling the sample stage. These experiments indicate that the low temperature limit to the acetic-acid water-based diamond deposition process appears to be between 200°C and 250°C. The quality of the diamond, once again, does not appear to degrade as the temperatures is reduced below 300°C. However, at 200°C, no carbon deposition occurred. It is yet to be determined if this result is a nucleation problem or a deposition problem.

Acknowledgements: The authors gratefully acknowledge the support of this work by the SDIO/IST through ONR (Contract No. N00014-92-0081).

1) R.A. Rudder, G.C. Hudson, J.B. Posthill, R.E. Thomas, R.C. Hendry, D.P. Malta, R.J. Markunas, T.P. Humphreys, and R.J. Nemanich, Appl. Phys. Lett., **60** , 329 (1992).

2) R.A. Rudder, J.B. Posthill, G.C. Hudson, D.P. Malta, R.E. Thomas, R.J. Markunas, T.P. Humphreys, and R.J. Nemanich, Mater. Res. Soc. Symp. Proc., **242**, 23 (1992).

3) R.K. Singh, D. Gilbert, R. Tellshow, R. Koba, R. Ochoa, J.H. Simmons, P.H. Holloway, J. Rodgers, and K. Buckle, Mater. Res. Soc. Symp. Proc., **31** (1992).

4) Shu Jin and T.D. Moustakas, Diamond 1992 Abstract # 8.69, August 31-September 4, 1992, Heidelberg, Germany.

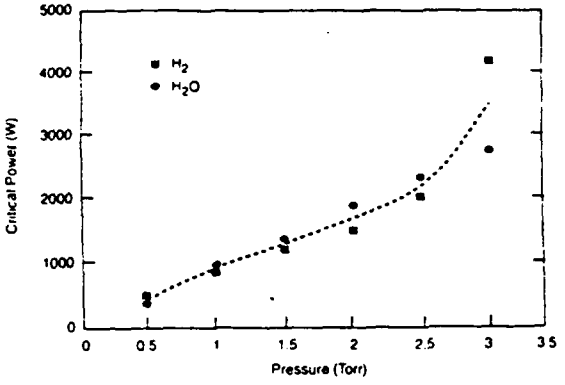

Fig. 1. Critical Power Necessary for Induction Coupling for Pure Water and Pure Hydrogen Discharges.

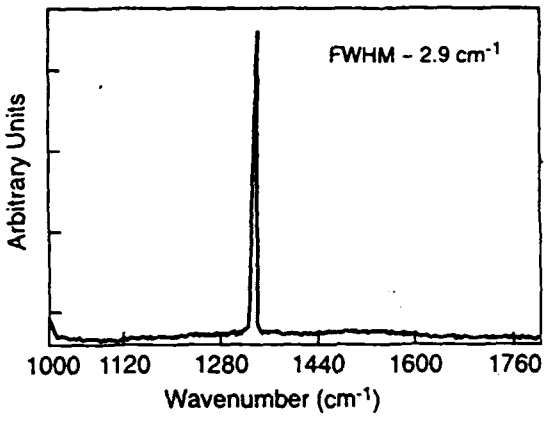

Fig. 3. Micro-Raman Spectrum from the Diamond Crystals Shown in Figure 2.

Fig. 2. SEM Micrographs of Discrete Diamond Particles Deposited at 250 °C from Acetic Acid:Water:Methanol.

INVITED TALK

Meeting: **1992 TMS Fall Meeting, Chicago, IL**
Symposium: **Beam Processing of Advanced Materials**

NUCLEATION OF DIAMOND FILMS ON NON-NATIVE SUBSTRATES

J.B. Posthill, R.A. Rudder, D.P. Malta, R.E. Thomas, G.C. Hudson, and R.J. Markunas, *Research Triangle Institute, Research Triangle Park, NC 27709.*

Different materials have been examined for their intrinsic propensity for nucleation of diamond from the vapor phase. Certain standard and unconventional sources have been employed to grow diamond in an rf-driven plasma-enhanced CVD system. These include: (1) CH_4/H_2, (2) CO/H_2, (3) CF_4/H_2, and (4) alcohol/H_2O-based mixtures. It has been found that diamond heteronucleation can be radically affected by the specific growth chemistry as well as the identity of the substrate material. For example, CF_4/H_2 mixtures have been found to nucleate diamond on Si(100) without the need for any substrate pretreatment. An amorphous interlayer has been observed between the diamond film and single crystal Si. Using a more conventional mixture of CH_4/H_2, we have achieved nucleation and growth of diamond with complete coverage and well-faceted topography on sintered cubic BN compacts without any surface pretreatment. These and other results will be discussed in the context of the interplay between different gas phase chemistries and different substrates used for diamond heteronucleation.